Application of Artificial Intelligence Methods in Geosciences and Hydrology

Chapter: Application of Fuzzy Inference System to Estimating Rock Properties from Well Logs and Seismic Data for groundwater level prediction

Edited by: Ata allah Nadiri

Published Date: December, 2015

Published by **OMICS Group eBooks**

731 Gull Ave, Foster City, CA 94404, USA

A free online edition of this book is available at www.esciencecentral.org/ebooks

Additional hard copies can be obtained from orders @ www.esciencecentral.org/ebooks

ISBN: 978-1-63278-061-4-03
DOI: http://dx.doi.org/10.4172/978-1-63278-061-4-062

Application of Fuzzy Inference System to Estimating Rock Properties from Well Logs and Seismic Data

Ali Kadkhodaie-Ilkhchi*[1,2]

[1]Department of Geology, Faculty of Natural Science, University of Tabriz, Iran

[2]Department of Petroleum Engineering, School of Chemical and Petroleum Engineering, Faculty of Science and Engineering, Curtin University of Technology, Perth, Western Australia

***Corresponding author:** Ilkhchi Department of Geology, Faculty of Natural Science, University of Tabriz, Iran, Department of Petroleum Engineering, School of Chemical and Petroleum Engineering, Faculty of Science and Engineering, Curtin University of Technology, Perth, Western Australia. E-mails: Kadkhodaie_ali@tabrizu.ac.ir & ali.kadkhodaie@curitn.edu.au

Introduction

Fuzzy inference system is the process of formulating the mapping from a given input to an output using fuzzy logic. The mapping then provides a basis from which decisions can be made, or patterns discerned. The basic concept of fuzzy logic, or fuzzy set theory, was first introduced by Lotfi Zadeh in 1965 at the University of California, Berkeley. Fuzzy logic is an extension of conventional Boolean logic (zeros and ones) developed to handle the concept of "partial truth" - truth values between "completely true" and "completely false". Science is heavily influenced by Aristotle's laws of logic initiated by the ancient Greeks and developed by many scientists and philosophers since. Aristotle's laws are based on "X or not-X"; a thing either is, or is not. This has been used as a basis for almost everything that we do. We use it when we classify things and when we judge things [1]. Managers want to know whether it is this or that, and even movies have clear goodies and baddies. Conventional logic is an extension of our subjective desire to categorise things. Life is simplified if we think in terms of black and white. This way of looking at things as true or false was reinforced with the introduction of computers that only use bits 1 or 0. When the early computers arrived with their machine driven binary system, Boolean logic was adopted as the natural reasoning mechanism for them. Conventional logic forces the continuous world to be described black and white, but in shades of grey. Not only does truth exist on a sliding scale, but also because of the uncertainty in measurements and interpretations, a grey scale can be a more useful explanation than two end points. For instance, we can look at a map of the earth and see mountains and valleys, but it is difficult to define where mountains start and the valleys end. This is the mathematics of fuzzy logic. Once the reality of the grey scale has been accepted, a system is required to cope with the multitude of possibilities. Probability

Application of Artificial Intelligence Methods in Geosciences and Hydrology
Edited by: Ata Allah Nadiri

theory helps quantify the greyness or fuzziness. It may not be possible to understand the reason behind random events, but fuzzy logic can help bring meaning to the bigger picture.

Early investigators of natural science noticed that many seemingly random events fell into a pattern. These eighteenth century scientists found an astonishing degree of regularity in the variation of an observation about its mean or average value. These patterns or distributions were closely approximated by continuous curves referred to “normal curves of errors” and attributed to the laws of chance. These curves are now called normal or Gaussian curves and have a characteristic bell shape. This distribution is the cornerstone of modern statistical theory [2].

The normal distribution is more than an accident of nature. It is a fundamental result of applied probability known as the Central Limit Theorem. This remarkable theorem states that a distribution that is the result of a number of underlying, relatively independent, variables will be normal in shape irrespective of the distribution shapes of the component variables. For instance if we take the porosity of a core-plug, each plug consists of numerous pores, each of which contribute to the pore volume. Many factors control an individual pore volume including grain shape, mineralization and pore fluids. In addition, when we measure porosity the resulting errors are the combined effect of a large number of independent sources of error. The resulting porosity distribution will be normal as a direct result of the Central Limit Theorem and this is confirmed by the empirical analysis of core-plugs.

Fuzzy logic does not require a normal distribution to work as any type of distribution that can be described can be used. Because of the prevalence of the normal distribution, supported by the Central Limit Theorem and observation, it is the best distribution to use in most cases. The normal distribution is completely described by two parameters, its mean and variance. As a consequence, core-plugs from a particular lithofacies may have dozens of underlying variables controlling their porosities but their porosity distribution will tend to be normal in shape and defined by two parameters - their average value or mean and their variance or the width of the distribution. This variance (the standard deviation squared) depends on the hidden underlying parameters and measurement error. This variance, or fuzziness, about the average value, is a key to the method and the reason why it is called fuzzy logic. Take, for instance, a piece of reservoir rock. Aeolian rock generally has good porosity and fluvial rock poorer porosity. If we find a piece of rock with a porosity of 2 Porosity Units (pu) is it aeolian or fluvial? We could say it is definitely fluvial and get on with more important matters. But let’s say it is probably fluvial but there is a slim probability that it could be aeolian. Aeolian rocks are generally clean and fluvial rocks shalier. The same piece of rock contains 30% clay minerals. Is it aeolian or fluvial? We could say it is equally likely to be aeolian or fluvial based on this measurement. This is how fuzzy logic works. It does not accept it is either this or that. It assigns a greyness, or probability, to the quality of the prediction on each parameter of the rock, whether it is porosity, shaliness or colour. There is also the possibility that there is a measurement error and the porosity is 20 pu not 2 pu. Fuzzy logic combines these probabilities and predicts that based on porosity, shaliness and other characteristics, the rock is most likely to be aeolian. Fuzzy logic says that there is also the possibility it could be fluvial. In essence, fuzzy logic maintains that any interpretation is possible but some are more probable than others. One advantage of fuzzy logic is that we never need to make a concrete decision. What’s more, fuzzy logic can be described by established statistical algorithms; and computers, which themselves work in ones and zeros, can do this effortlessly for us [1].

From the exploration to development and production stages in a hydrocarbon reservoir, the engineering parameters embody a high level of uncertainties. Uncertainty defined as the gap between the present stage of knowledge and certainty. It is believed that petroleum reservoir data, including dynamic (e.g. pressure and hydrocarbon production) and static data (e.g. porosity and permeability), are inherently uncertain. More information on this can be found in Nikolaidsis (2005), Zoveidavianpoor and Gharibi (2015)[3,4]. Therefore,

definitions in petroleum related disciplines are not clear-cut and most of the time, are associated with uncertainties. Regarding to imprecise nature of fuzzy sets, it is appropriate to use fuzzy reasoning for solving problems which accompany vagueness and imperfection [5]. Conventional techniques try to minimize or ignore the error in predictions. Fuzzy logic asserts that there is useful information in this error. The error information can be used to provide a powerful predictive tool for the geoscientist to complement conventional techniques. In addition to fuzzy systems there are other methods which can deal with uncertainty in reservoir data such as adaptive neuro-fuzzy inference system and a committee of experts which is called as committee machines. The main cons and pros of the most popular artificial intelligence methods are listed in Table 2.1

Method	Strong points	Weak points
Neural networks	NNs are fast, robust and easily trained. They can approximate functions with high degree of non-linearity.	Optimization algorithms may fall in local minima, parameters setting is tedious as number of hidden layers and neurons increase.
Fuzzy Logic	Assess uncertainty in data and use the error in data as an estimator tool	In most cases fuzzy systems are fail to deal with problem with high degree of non-linearity
Neuro-Fuzzy	Reaps the benefits of both neural networks and fuzzy inference system	Converges late and may fall in local minima

Table 2.1: Cons and pros of the popular artificial intelligence methods.

Application of Fuzzy Inference for Rock Properties Estimation

The last decade has witnessed significant advances in the study and application of fuzzy systems in the petroleum industry. The establishment of the existence of an intelligent formulation, between two sets of data (inputs/outputs), has been the main topic of such studies. One such topic, of great interest, was to characterize how well log and seismic data can be related to lithology, rock types, fluid content, porosity, shear wave velocity and other reservoir properties. Petrophysical parameters, such as water saturation and porosity, are very important data for hydrocarbon reservoir evaluation and characterization.In this chapter, some of the recent applications of fuzzy inference systems in petroleum industry are reviewed.

Synthesis of Well Log Data

Petrophysical logs are one of the most important tools for the evaluation of hydrocarbon reservoirs. Parameters such as porosity, volume of shale, formation water saturation, lithology, fluid contacts and productive zones are obtained from well logs. In many cases, a complete set of log data may not be available-hole conditions, instrument failure, loss of data due to inappropriate storage and incomplete loggings are some of the reasons. Rezaee et al. (2008) [6] used a Takagi–Sugeno fuzzy interference system (TS-FIS*)* for creating synthetic petrophysical logs. The petrophysical data including neutron (NPHI), density (RHOB), sonic (DT) and deep resistivity (LLD) from two wells were used for constructing intelligent models in the Fahliyan limestone reservoir, the Persian Gulf. A third well from the field was used to evaluate the reliability of the models. The well log data were acquired in 1982 by Schlumberger Well Services Co.; the reservoir is predominantly limestone and the play type is oil. For each of the constructed models, the data sets were divided into two groups including the modelling data (1986 data points) from two wells and the test data (748 data points) from the third well. Appropriate inputs to construct intelligent models based on *FL* are determined from crossplot analysis (Table 2.2) of log data from the two wells (known inputs). All input and output membership functions and their parameters were extracted by a subtractive clustering method and then a set of fuzzy 'if–then' rules were generated for the formulation of input data of the target well log.

Synthesized Log	NPHI	RHOB	DT	LLD
Inputs	DT, RHOB	NPHI, DT	NPHI, RHOB	LLS, MSFL, NPHI

Table 2.2: Appropriate inputs for synthesizing wireline logs (6].

In the first step, it is necessary to obtain the best type of membership functions (MFs) and an optimal number of *MFs* and fuzzy if–then rules. Too few rules cannot cover the entire domain completely, and too many may complicate the system, causing low performance of the model.

Membership function types were determined by fitting the proper function to the distribution of the used well log data in the studied reservoir. For this purpose, several frequency plots were generated showing the distribution of the data. Then, the best membership functions were fitted to the generated plots. A subtractive clustering was used to extracting the optimal number of rules and *MFs*. In subtractive clustering each data point, not a grid point, is considered as a potential cluster centre. Using this method, the number of effective "grid points" to be evaluated is simply equal to the number of data points, independent of the dimension of the problem. Another advantage of this method is that it eliminates the need to specify a grid resolution, in which tradeoffs between accuracy and computational complexity must be considered.

The Subtractive Clustering Algorithm

The subtractive clustering method works as follows. Consider a collection of n data points $\{x_1,x_2,\ldots,x_n\}$ in an M dimensional space. Without loss of generality, we assume that the data points have been normalized in each dimension so that they are bounded by a unit hypercube. We consider each data point as a potential cluster centre and define a measure of the potential of data point x_i as [7]:

$$P_i = \sum_{j=1}^{n} e^{-\alpha \|x_i - x_j\|^2} \qquad \text{(Eq. 2.1)}$$

Where $\alpha = 4/r_a^2$,

$||.||$ denotes the Euclidean distance, and r_a is a positive constant. Thus, the measure of the potential for a data point is a function of its distances to all other data points. A data point with many neighbouring data points will have a high potential value. The constant r_a is effectively the radius defining a neighbourhood; data points outside this radius have little influence on the potential.

After the potential of every data point has been computed, we select the data point with the highest potential as the first cluster centre. Let x_1^* be the location of the first cluster centre and P_1^* be its potential value. We then revise the potential of each data point x_i by the formula.

$$P_i \Leftarrow P_i - P_1^* e^{-\beta \| x_i - x_1^* \|^2} \qquad \text{(Eq. 2.2)}$$

Where $\beta = 4/r_b^2$

And r_b is a positive constant. Thus, we subtract an amount of potential from each data point as a function of its distance from the first cluster centre. The data points near the first cluster centre will have greatly reduced potential, and therefore will unlikely be selected as the next cluster centre. The constant r_b is effectively the radius defining the neighbourhood which will have measurable reductions in potential. To avoid obtaining closely spaced cluster centres, we set r_b to be somewhat greater than r_a ; a good choice is $r_b = 1.25\ r_a$.

When the potential of all data points has been revised according to Eq. (2.2), we select the data point with the highest remaining potential as the second cluster centre. We then further reduce the potential of each data point according to their distance to the second cluster centre. In general, after the k^{th} cluster centre has been obtained, the potential of each data point is revised by the Eq. (2.3)

$$P_i \Leftarrow P_i - P_k^* e^{-\beta |x_i - x_k^*|^2} \quad \text{Eq. (2.3)}$$

Where x^*_k is the location of the k^{th} cluster centre and P^*_k is its potential value.

The process of acquiring new cluster centre and revising potentials repeats until the remaining potential of all data points falls below some fraction of the potential of the first cluster centre P^*_1. In addition to this criterion for ending the clustering process are criteria for accepting and rejecting cluster centres that help avoid marginal cluster centres. The following criteria are used:

If $P_k^* \rangle \eta P_1^*$

Accept x^*_k as a cluster center and continue.

else if $P_k^* \langle \varepsilon P_1^*$

Reject x^*_k and end the clustering process.

else

Let d_{min} = shortest of the distances between

x^*_k and all previously found cluster centers.

If $\frac{d_{\min}}{r_a} + \frac{P^*_k}{P^*_1} \geq 1$

Accept x^*_k as a cluster centre and continue.

else

Reject x^*_k and set the potential at x^*_k to 0.

Do not revise the potential of other data points.

Select the data point with the next highest potential as the new x^*_k and re-test.

end if

end if

Here η specifies a threshold for the potential above which we will definitely accept the data point as a cluster centre; ε specifies a threshold below which we will definitely reject the data point. Good default values are η = 0.5 and ε = 0.15. If the potential falls in the gray region, we check if the data point offers a good trade-off between having a sufficient potential and being sufficiently far from existing cluster centres [7].

In this study, by specifying a set of values for the clustering radius which differs between 0 and 1, several numbers of rules were generated. Then, the Mean Square Error *(MSE)* of the generated models was measured and the models with the highest performance (lowest error) were chosen as the optimal fuzzy inference systems for generating petrophysical logs. Here, the generated *MFs* and fuzzy 'if–then' rules for synthesizing sonic log are as below:

Neutron log: By specifying 0.25 for the clustering radius, four Gaussian type membership functions were extracted for DT and RHOB inputs which were classified as very low, low, moderate and high. Generated 'if–then' rules are below (figure 2.1):

(1) If (DT is very low) and (RHOB is high) then (NPHI is very low).

(2) If (DT is low) and (RHOB is moderate) then (NPHI is low).

(3) If (DT is moderate) and (RHOB is low) then (NPHI is moderate).

(4) If (DT is high) and (RHOB is very low) then (NPHI is high).

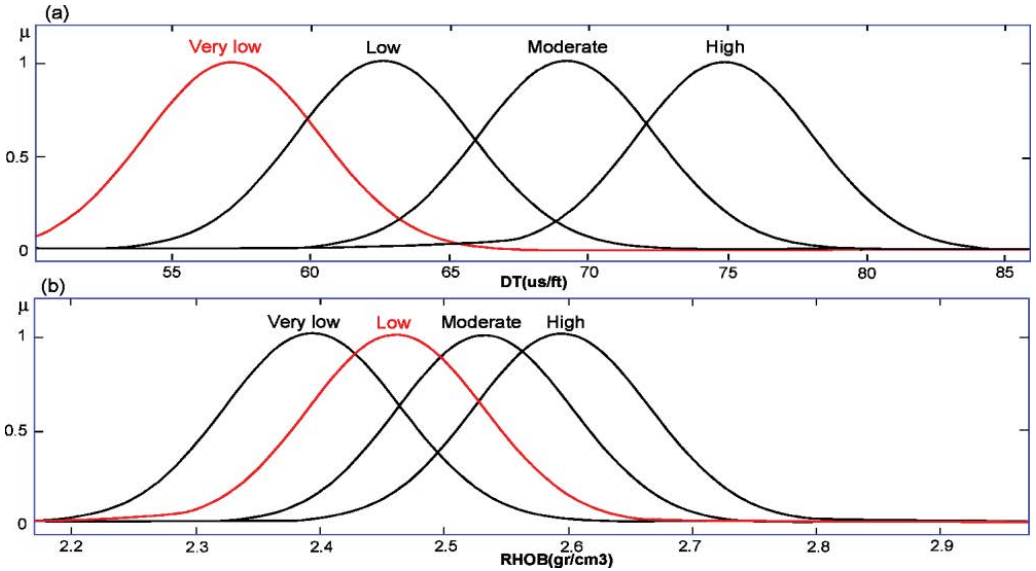

Figure 2.1: DT and RHOB membership functions for synthesizing NPHI log [6].

Density log (RHOB): By specifying 0.5 for the clustering radius, three Gaussian type membership functions were extracted for NPHI and DT inputs which were classified as low, moderate and high (figure 2.2). Generated 'if–then' rules are below:

(1) If (NPHI is low) and (DT is low) then (RHOB is high).

(2) If (NPHI is moderate) and (DT is moderate) then (RHOB is moderate).

(3) If (NPHI is high) and (DT is high) then (RHOB is low).

Sonic log: By specifying 0.5 for the clustering radius, three Gaussian type membership functions were extracted for NPHI and RHOB inputs which were classified as low, moderate and high (figure 2.3). Generated *if–then* rules are as below:

(1) If (NPHI is low) and (RHOB is high) then (DT is low).

(2) If (NPHI is moderate) and (RHOB is moderate) then (DT is moderate).

(3) If (NPHI is high) and (RHOB is low) then (DT is high).

Deep laterolog. By specifying 0.65 for the clustering radius, three Gaussian type membership functions were extracted for LLS, MSFL and NPHI inputs which were classified as low, moderate and high (figure 2.4). Generated 'if–then' rules are as below:

(1) If (LLS is low) and (MSFL is low) and (NPHI is high) then (LLD is low).

(2) If (LLS is moderate) and (MSFL is moderate) and (NPHI is moderate) then (LLD is moderate).

(3) If (LLS is high) and (MSFL is high) and (NPHI is low) then (LLD is high).

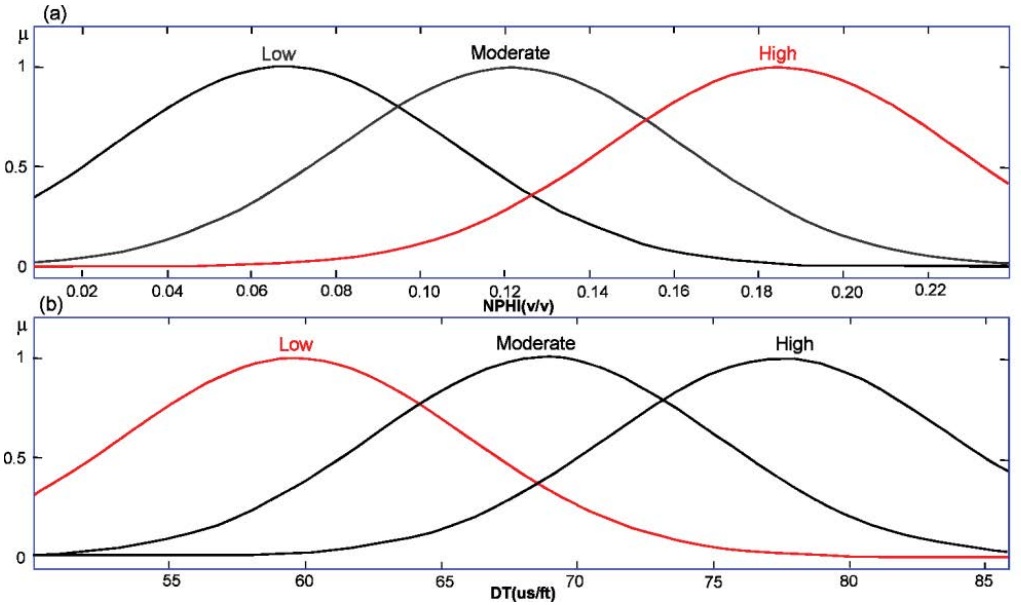

Figure 2.2: NPHI and DT membership functions for synthesizing RHOB log .

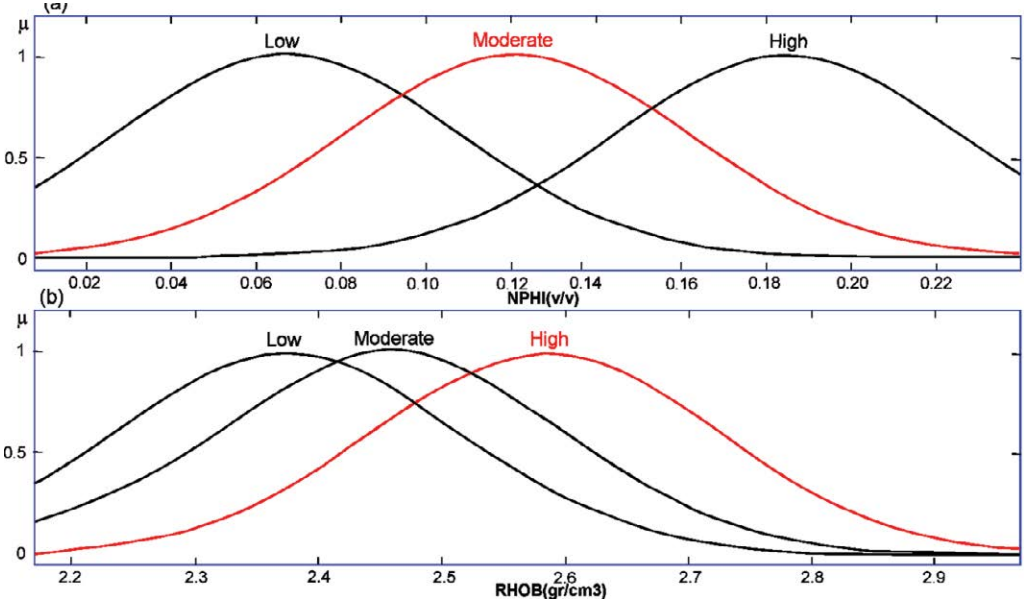

Figure 2.3: NPHI and RHOB membership functions for synthesizing DT log [6].

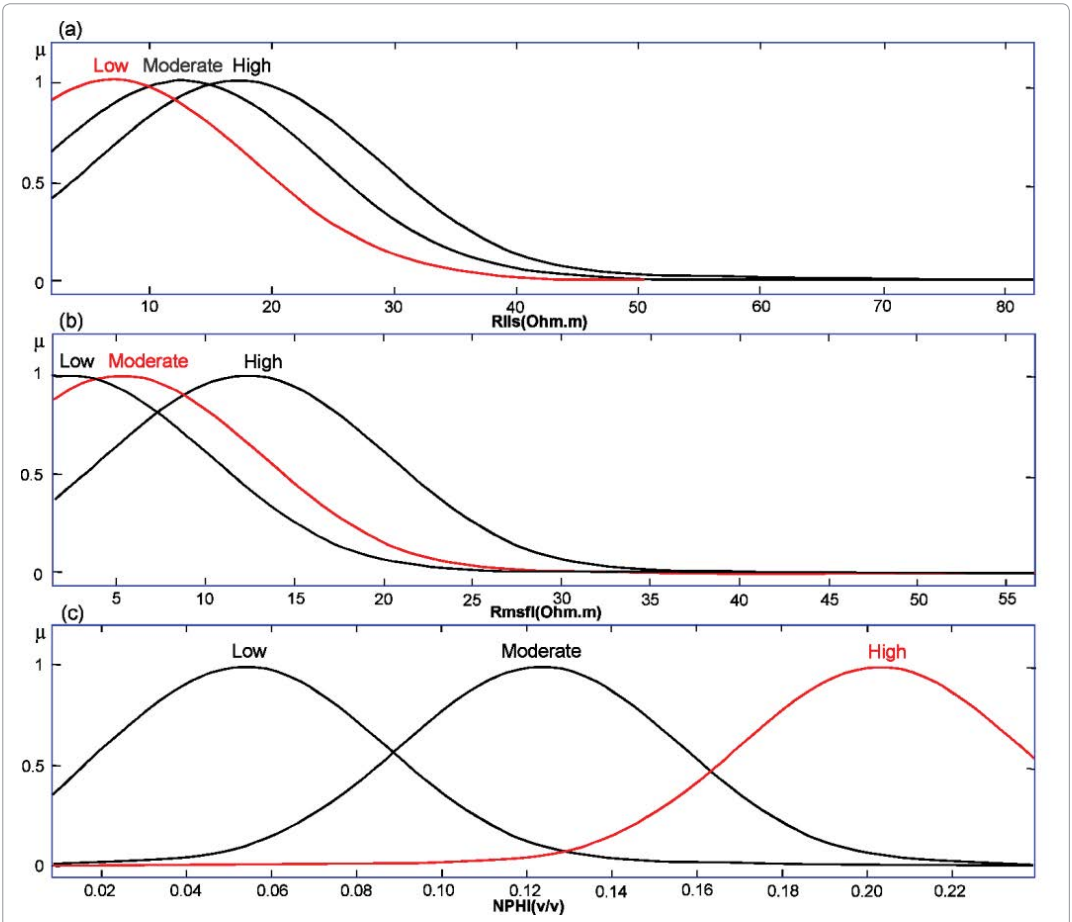

Figure 2.4: LLS, MSFL, and NPHI membership functions for synthesizing LLD log [6].

After preparation of fuzzy models, following steps were carried out for the estimation of log values in the third well of the field by using FIS [8]:

Step 1. Fuzzify inputs: The FIS takes the inputs and determines the degree to which the inputs belong to each membership function.

Step 2. Apply fuzzy operator and truncation method: For the case that the antecedent of a given rule has more than one part, the fuzzy operator is applied to obtain one rule that represents the result of the antecedent for that rule. The most common operators are shown below:

"AND"= use the minimum of the options.
"OR" = use the maximum of the options.
"NOT" = use 1- option

Applying the fuzzy operators gives a value to the antecedent of each rule, and then the output membership function is truncated by this value. In this study "AND" has been used.

Step 3. Apply aggregation method: In this step, outputs of each rule that fit into a fuzzy set are combined into a single fuzzy set.

Step 4. Defuzzify: The input for defuzzification process is the results of aggregation method. Then FIS uses a defuzzification method (in this study, a weighted average) for the resulting output which is a crisp numerical value. Figure 2.5 shows an example of fuzzy

rules and processing steps to use *TS-FIS* for creation of sonic log from neutron and density log inputs. Measured *MSE* for FL predicted NPHI, RHOB, DT, and GR in the test well was equal to 0.134, 0.128, 0.122, and 0.091, respectively.

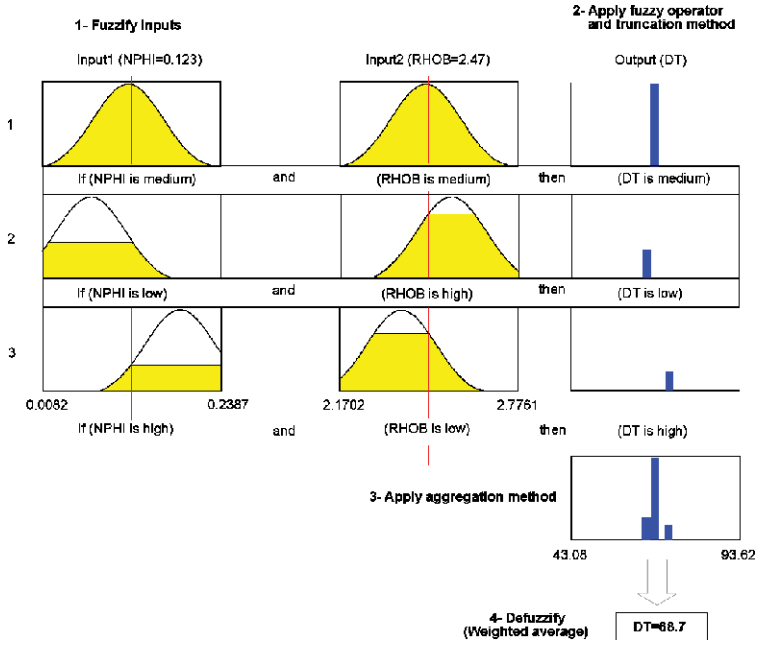

Figure 2.5: Processing steps in using *TS-FIS* for creation of a sonic log from neutron and density log inputs. This FIS consists of three rules with the antecedent of each rule separated by the 'and' operator [6].

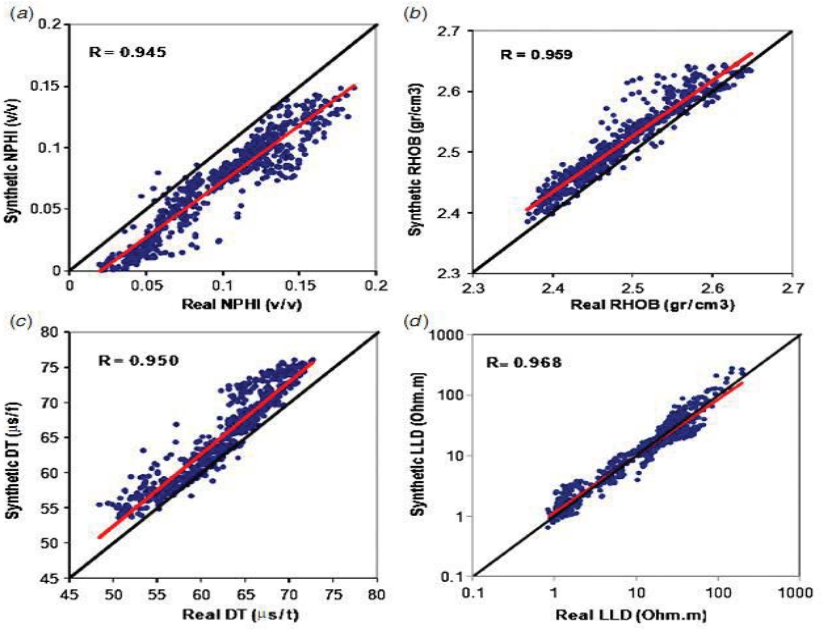

Figure 2.6: Crossplots showing the correlation coefficient for synthesizing (a) NPHI, (b) RHOB, (c) DT and (d) LLD logs utilizing *FL* for the test well [6].

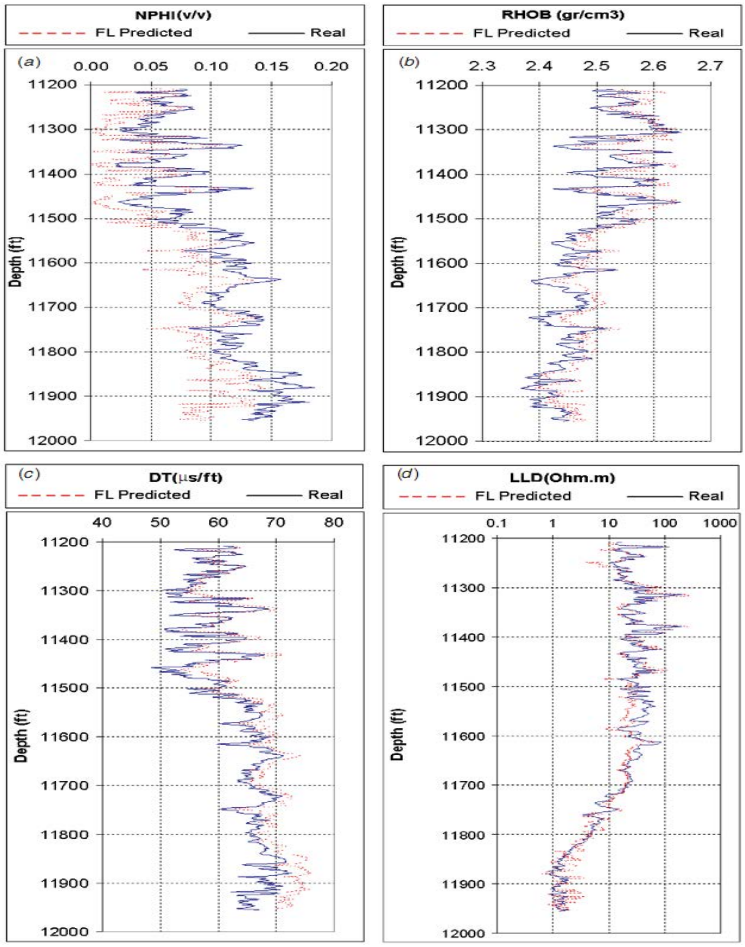

Figure 2.7: Crossplots showing the correlation coefficient for synthesizing (a) NPHI, (b) RHOB, (c) DT and (d) LLD logs utilizing *FL* for the test well [6].

Permeability Estimation from Well Log Data

Pore geometry is a key element that controls permeability.

When input data were selected, they were divided into two groups including modelling data (1076 data points) from three wells (A, B and C) and test data (125datapoints) from the forth well (D). All membership functions and their parameters were extracted by a subtractive clustering method. By specifying 0.65 for the clustering radius, three Gaussian-type membership functions were extracted for used inputs which were captioned by low, moderate, and high.

The algorithm of fuzzy rules extraction is explained as follows:

The input data for fuzzy rules generation are cluster centres extracted using any fuzzy clustering approach. The methodology for construction of fuzzy rule base using the cluster centre is described as follows. For a set of m cluster centres $\{u_1, u_2,..., u_m\}$ in an M dimensional space we assume that the first N dimensions correspond to input variables and the last M-N dimensions correspond to output variables. Each vector u_i could be decomposed into two component vectors v_i (inputs) and w_i(outputs). We consider each cluster centre u_i as a fuzzy

rule that describes the system behaviour. Intuitively, each cluster centre represents the rule (Chiu, 1995 & 1997)[10,11]:

Rule i : If {input is near v_i } then output is near w_i .

Given an input vector x_0, the degree of fulfilment of rule *i* is defined as Eq. (2.4)

$$\tau_i = e^{-\lambda \|x_0 - v\|^2} \qquad \text{(Eq. 2.4)}$$

Where λ is the constant. The output vector *z* is calculated via Eq. (2.5)

$$z = \left[\sum_{i=1}^{m} \tau_i w_i\right] \div \left[\sum_{i=1}^{m} \tau_i\right] \qquad \text{(Eq. 2.5)}$$

This computational model corresponds to the MFIS and LFIS employing traditional fuzzy if-then rules. Each rule has the following form:

if $input_1$ is Ai_1 & $input_2$ is A_{i2} & ... then $output_1$ is C_{i1} & $output_2$ is C_{i2} ...

where $input_j$ is the j^{th} input variable and $output_j$ is the j^{th} output variable; A_{ij} is an exponential membership function in the i^{th} rule associated with the j^{th} input and B_{ij} is a membership function in the i^{th} rule associated with the j^{th} output. For the i^{th} rule, which is represented by cluster center u_i, A_{ij} is given by Eq. (2.6)

$$A_{ij}(Y_j) = exp(-1/2(input_j - v_{ij})/\sigma_{ij})^2) \qquad \text{(Eq. 2.6)}$$

and C_{ij} can be any symmetric membership function centred around w_{ij}, where v_{ij} is the j^{th} element of v_i, w_{ij} is the j^{th} element of w_i, and σ^2_{ij} is the variance of cluster *i* in the j^{th} rule.

Fuzzy if-then rules for permeability estimation

Having the results of subtractive clustering following rules were used to formulate permeability to well log data (figure 2.8):

1. If (NPHI is low) and (DT is low) and (RHOB is high) and (GR is low) and (Rlld is low) then (permeability (K) is low).

2. If (NPHI is moderate) and (DT is moderate) and (RHOB is moderate) and (GR is moderate) and (Rlld is moderate) then (permeability (K) is moderate).

3. If (NPHI is high) and (DT is high) and (RHOB is low) and (GR is high) and (Rlld is high) then (permeability (K) is high).

The performance of the fuzzy model was measured as 0.0019 by using the mean squared error *(MSE)* function. A comparison of measured and predicted permeability versus depth is shown in figure 2.9.

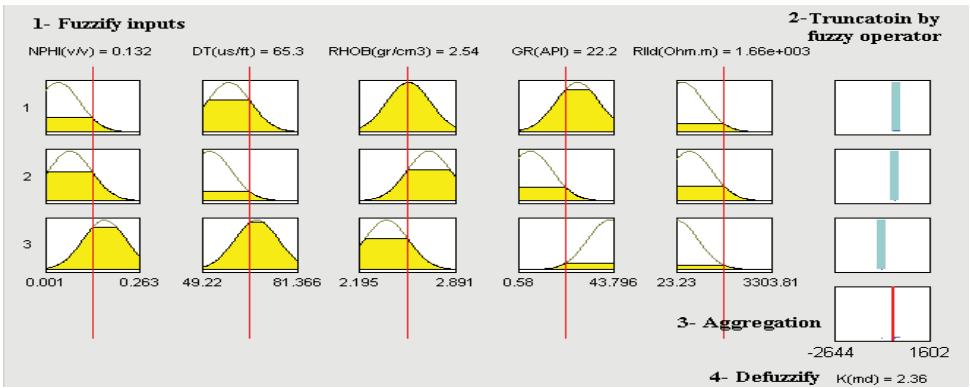

Figure 2.8: Formulation of petrophysical data to permeability using three fuzzy if-then rules [9].

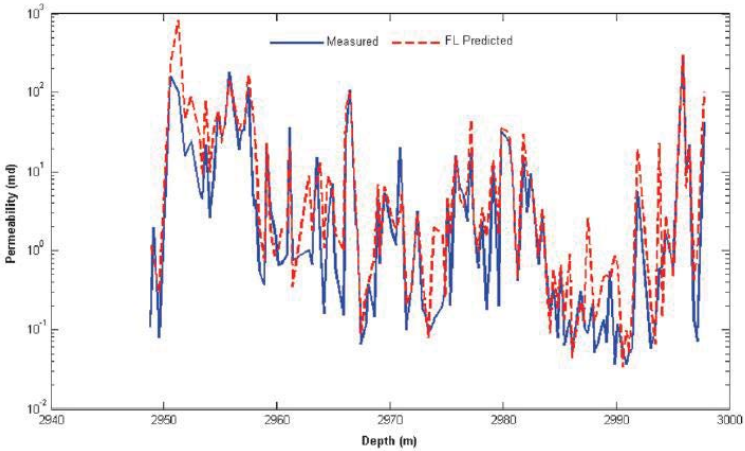

Figure 2.9: Formulation of petrophysical data to permeability using three fuzzy if-then rules [9].

Cuddy (1998)[1] applied the fuzzy mathematic to model permeability in the Ula field, Norway. The recoverable reserves of Ula are 435 million barrels of oil, 167 billion cubic feet of gas and 42.8 million barrels of *NGL*. The reservoir is late Jurassic sandstone at a depth of 3320 m tvdss. It has porosities of around 20 pu with average permeability of 300 md. Fuzzy logic was used to update the reservoir model in order to unlock the potential of an upper unit using new drilling techniques.This interval contains potentially 50% of the remaining reserves and was initially ignored because of poor rock characteristics. The right hand track of figure 2.10 shows the comparison between core derived and fuzzy predicted permeability in one of the cored Ula wells. "Blind-testing" between wells was used to test the predictive ability of the technique. To test the fuzzy prediction, the technique was calibrated in a cored well and "Blind-tested" in another well to see how well it fitted the actual core permeability. Figure 2.11 shows the second well where permeability were predicted using the calibration from the first well. The comparison between the predicted and cored derived permeability is good.

Other case studies for permeability and other reservoir properties estimation could be found Nikravesh and Aminzadeh (2003 & 2003) and Lim (2005)(12,13).

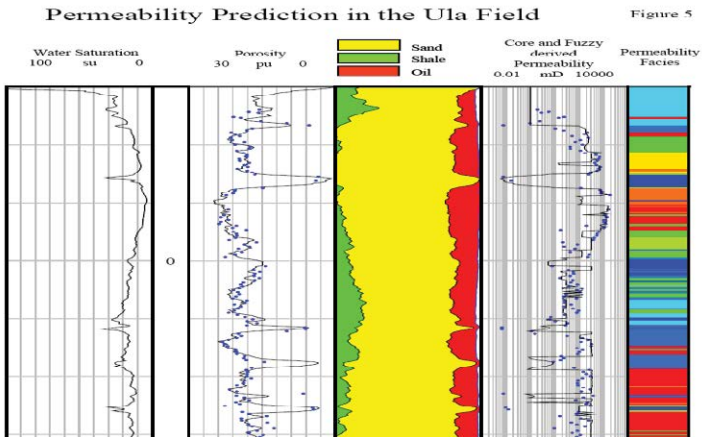

Figure 2.10: The comparison between core derived and fuzzy predicted permeability in one of the cored Ula wells [1].

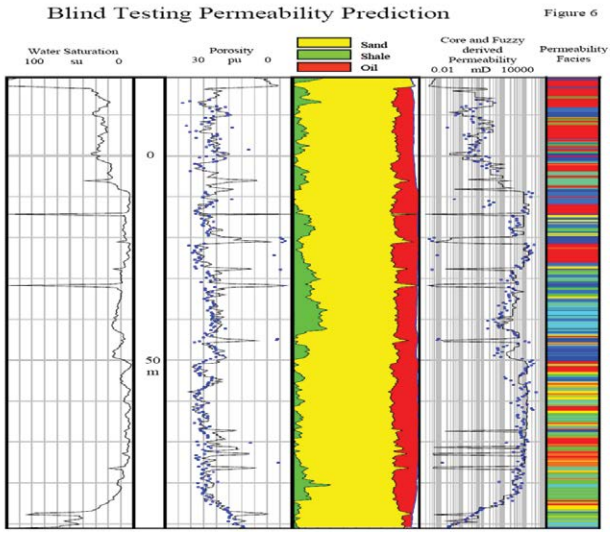

Figure 2.11: The second well where permeability were predicted using the calibration from the first well [1].

Shear Wave Velocity (Vs) Estimation

Shear wave velocity (Vs) associated with compressional wave velocity (Vp) can provide accurate data for geophysical study of a reservoir. These so called petroacoustic studies have important role in reservoir characterization objectives such as lithology determination, identifying pore fluid type, and geophysical interpretation. Rezaee et al. (2007)(5) designed a Takagi-Sugeno fuzzy model as an intelligent tool to predict Vs from conventional log data in a sandstone reservoir of the Carnarvon Basin, NW Shelf of Australia. The northern part of the Carnarvon Basin on the North West Shelf of Australia is one of the most prospective petroleum provinces in the country. The sub-basin occupies an area about 100 km × 200 km (20,000 km2), that covers the offshore from the Monte Bello Islands in the north to the Onslow town in the south. The shear velocity data only exist in some intervals of Bay #1, Emperor #1 and East_Spar #4 AST1 wells. The log data of first two wells including sonic log, gamma ray (GR), deep laterolog resistivity (Rlld), bulk density (FDC) and neutron porosity (NPHI) were used to construct intelligent models. The third well (East_Spar#4) was used to evaluate the reliability of the models. Their results showed that there is a good agreement between measured and fuzzy estimated shear wave velocity (figure 2.13).

In their study, the optimum number of rules and MFs were extracted by using a subtractive clustering (clustering radius= 0.5). Four rules associated with four Gaussian type membership functions were generated for each of the input data set which were captioned by low, moderate, high, and very high, respectively:

1) If (Vp is very high) and (GR is high) and (Rlld is Moderate) and (FDC is high) and (NPHI is moderate), then (Vs is very high).

2) If (Vp is moderate) and (GR is low) and (Rlld is high) and (FDC is low) and (NPHI is low), then (Vs is moderate).

3) If (Vp is high) and (GR is very high) and (Rlld is low) and (FDC is very high) and (NPHI is very high), then (Vs is high).

4) If (Vp is low) and (GR is moderate) and (Rlld is very high) an d (FDC is moderate) and (NPHI is high), then (Vs is low).

A graphical illustration showing formulation of conventional well log inputs to Vs using four fuzzy if-then rules is shown in figure 2.13.

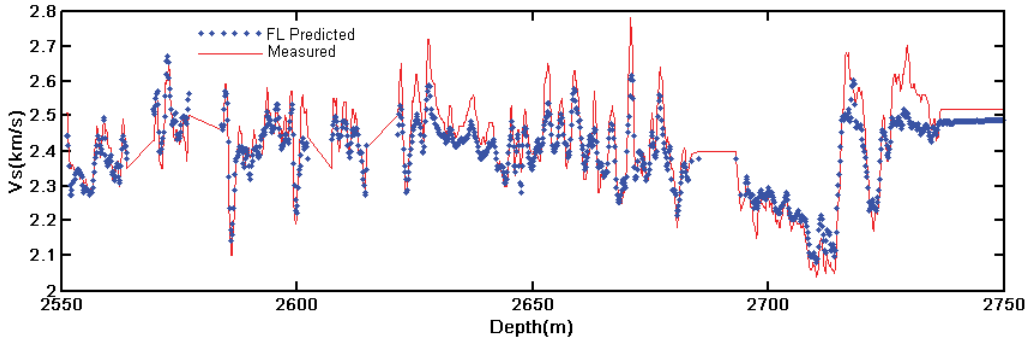

Figure 2.12: A comparison between measured and predicted Vs using fuzzy inference system for the test well East Spar#4 AST1. Real values were shown by solid lines and predicted values by dotted lines [5].

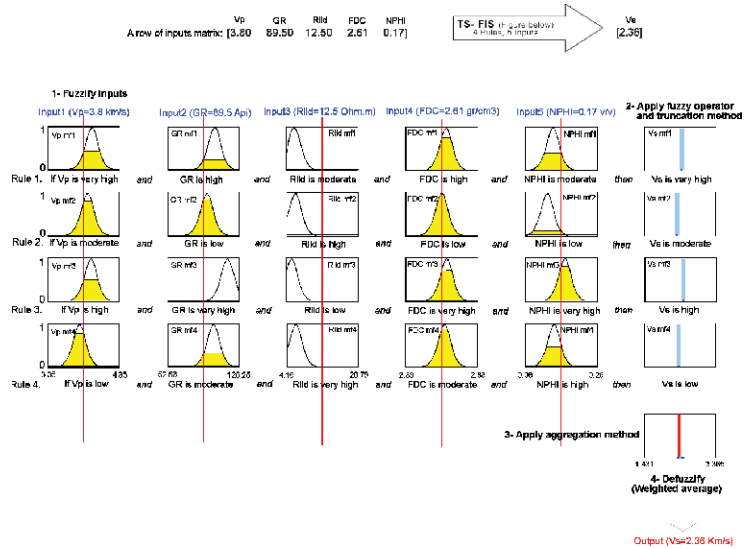

Figure 2.13: A graphical illustration showing formulation of conventional well log inputs to Vs using four fuzzy if-then rules generated by TS-FIS. Each input is covered by four Gaussian membership functions (for example, Vp mf1, Vp mf2, Vp mf3, Vp mf4 which are captioned by very high, high, moderate, and low, respectively). By passing a row of the inputs matrix including Vp = 3.8 Km/s, GR = 89.5 API, Rlld = 12.5 Ohm.m, FDC = 2.61 gr/cm^3, and NPHI= 0.17 (p.u.) from the FIS, its related MFs are affected in each rule. For example, the Vp value of 3.8 will affect the Vp mf1, Vp mf2, Vp mf3, and Vp mf4 to the degrees (grade of membership) that are shown by the height of yellow colour. This procedure will be done for entire inputs to each rule. Because the antecedent of each rule has more than one part, the fuzzy "and" operator is applied to obtain one rule that represents the result of the antecedent for that rule. Applying the fuzzy operators gives a value to the antecedent of each rule, and then the output membership function is truncated by this value. Then outputs of each rule that fit into a fuzzy set are combined into a single fuzzy set (aggregation). Finally, FIS uses a weighted average method (defuzzify) for the resulting Vs which is a crisp numerical value. This process is repeated for other rows of inputs matrix [5].

Synthesis of Virtual *NMR* Logs

Nuclear Magnetic Resonance (NMR) log provides useful information for petrophysical study of the hydrocarbon bearing intervals. Free fluid porosity (effective porosity), rock permeability and Bound Fluid Volume (BFV) could be obtained by processing and interpretation of NMR data. Labani et al. (2010)[14] proposed an improved strategy to make a quantitative correlation between the *NMR* log parameters and conventional well logs using a Takagi-Sugeno fuzzy inference system in the South Pars gas field (figure 2.14). The Iranian

part of South Pars Gas Field, the world's largest non-associated gas accumulation, is located in the Persian Gulf, between Qatar and Iran at about 100 km from the Iranian shoreline. This field was discovered in 1990 by NIOC. It along with North Dome field cover some 9700 square Km^2 kilometers (North Dome) are in Qatari territorial waters. The estimates for the Iranian section are 500 tcf (14.2 tcm) of gas in place and around 360 tcf (10.1 tcm) of recoverable gas which stands for 36% of Iran's total proven gas reserves and 5.6% of the worlds proven gas reserves. The estimates for the Qatari section are 900 tcf (25.5 tcm) of recoverable gas which stands for almost 99% of Qatar's total proven gas reserves and 14% of the world's proven gas reserves [15].

The Upper Permian to Lower Triassic Dalan and Kangan Formations (equivalent of Khuff Formation) are the two main condensate and gas-bearing reservoirs units in this field. Kangan and Dalan reservoir rocks are divided into K5, Nar, K4, K3, K2 and K1 units

Figure 2.14: Location map of the South Pars Gas Field [15].

All input and output MFs and their parameters were extracted by a subtractive clustering method and then a set of fuzzy *if-then* rules were generated for formulation of the input data to the outputs. The optimum number of rules and MFs were extracted by specifying a set of values between 0 and 1 for clustering radius (Table 2.3) and then performance of the model was measured for the test well at each stage, the models with the highest performance (lowest error) were chosen as the optimal *FIS*.

Free fluid porosity (FFP)

By specifying 0.8 for the clustering radius, two Gaussian type MFs were extracted for inputs which were classified as low and high. The generated fuzzy 'if-then' rules for formulating input petrophysical data to FFP are as below (figure 2.15):

1. If (PHIE-HILT is low) and (NPHI is low) and (RHOZ is high) and (DT is low) then (FFP is low).

2. If (PHIE-HILT is high) and (NPHI is high) and (RHOZ is low) and (DT is high) then (FFP is high)

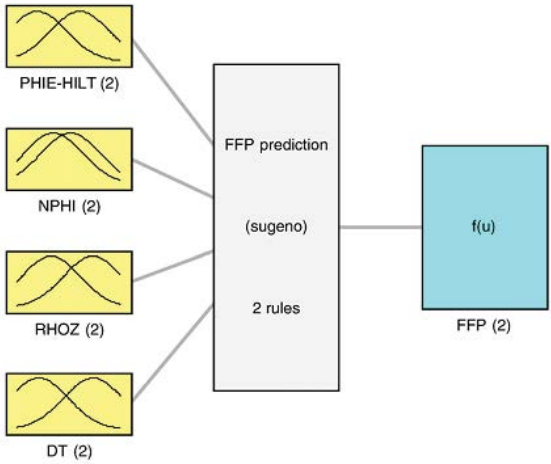

Figure 2.15: Formulation between inputs to output (FFP) using the TS-FIS [14].

NMR Permeability

By specifying 0.1 for the clustering radius, 8 Gaussian type MFs were extracted for inputs. Generated fuzzy 'if-then' rules are as below:

1. If (PHIE-HILT is mf1) and (NPHI is mf1) and (RHOZ is mf1) and (DT is mf1) then (permeability is mf1).
2. If (PHIE-HILT is mf2) and (NPHI is mf2) and (RHOZ is mf2) and (DT is mf2) then (permeability is mf2).
3. If (PHIE-HILT is mf3) and (NPHI is mf3) and (RHOZ is mf3) and (DT is mf3) then (permeability is mf3).
4. If (PHIE-HILT is mf4) and (NPHI is mf4) and (RHOZ is mf4) and (DT is mf4) then (permeability is mf4).
5. If (PHIE-HILT is mf5) and (NPHI is mf5) and (RHOZ is mf5) and (DT is mf5) then (permeability is mf5).
6. If (PHIE-HILT is mf6) and (NPHI is mf6) and (RHOZ is mf6) and (DT is mf6) then (permeability is mf6).
7. If (PHIE-HILT is mf7) and (NPHI is mf7) and (RHOZ is mf7) and (DT is mf7) then (permeability is mf7).
8. If (PHIE-HILT is mf8) and (NPHI is mf8) and (RHOZ is mf8) and (DT is mf8) then (permeability is mf8).

The measured mean squared errors (MSE) for the FL predicted FFP and permeability in the test well were equal to 0.000139 (pu)2 and 0.0197, respectively. The correlation coefficients (R^2) between the real data and FL predicted results for FFP and permeability are 0.881 and 0.862, respectively.

Correlation coefficient and agreement between measured and estimated *FFP* and *NMR* permeability is shown in figures 2.16 and 2.17.

No. FIS	Clustering Radius	No. of fuzzy 'if-then' rules		MSE of fuzzy model	
		FFP	Permeability	FFP $(pu)^2$	Permeability
1	0.1	16	8	0.000376	0.0196
2	0.2	7	4	0.000156	0.0228
3	0.3	7	2	0.000139	0.0210
4	0.4	4	2	0.000155	0.0203
5	0.5	4	1	0.000155	0.0235
6	0.6	4	1	0.000151	0.0235
7	0.7	3	1	0.000151	0.0235
8	0.8	2	1	0.000139	0.0235
9	0.9	2	1	0.000141	0.0235
10	1	2	1	0.000144	0.0235

Table 2.3: The *MSE* and number of fuzzy *if-then* rules for 10 *TS-FISs* generated by specifying a set of values between the range of [0, 1] for clustering radius [14].

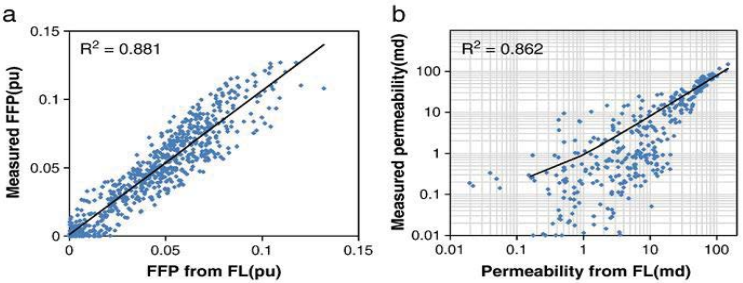

Figure 2.16: Crossplots showing the correlation coefficients between measured and *FL* predicted results for (a) FFP and (b) permeability [14].

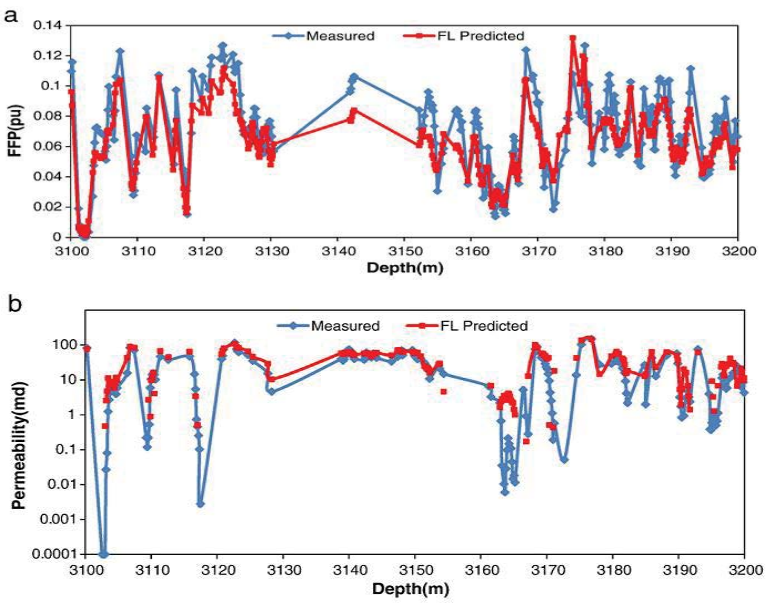

Figure 2.17: A comparison between measured and fuzzy predicted (a) FFP and (b) permeability versus depth in the test data [14].

Estimation of Total Organic Carbon

Total Organic Carbon (TOC*)* content present in reservoir rocks is one of the important parameters, which could be used for evaluation of residual production potential and geochemical characterization of hydrocarbon-bearing units. In general, organic-rich rocks could be characterized with the use of wireline logging data. Gamma ray tool measures the radioactivity of various formations. Generally, organic rich rocks have high concentrations of radioactive elements including Potassium, Thorium, and Uranium and increase the reading of gamma ray log. Neutron log reading is a response of hydrogen atoms concentration in rocks. The volume of organic matter in the formation has a direct relationship with hydrogen atoms content and porosity of the rock. Thus, neutron porosity increases in the organic rich intervals. The sonic transit time (DT) is the reciprocal of the velocity of the compressional wave and is a function of formation lithology, porosity, type and distribution models of fluids (water, gas, oil, kerogen, etc.). With apparent DT value increase *TOC* content tends to elevate [16]. Density log measures the bulk density of the formation, a response of fluids and matrix constituent minerals density. Organic matters have a low density (about 1 gr/cm3) and their concentration tends to reduce the bulk density of the rock.

Generally, organic matter bearing layers have higher resistivity than the other rocks. Specially, it is true when kerogen becomes mature and generates hydrocarbon filling pore spaces. Kadkhodaie et al. (2009a)[17] found a fuzzy relationship between gamma ray, neutron, sonic, density, resistivity logs and TOC data measured by Rock-Eval pyrolysis using a case study from the South Pars gas field. For this purpose, 124 samples from the logged intervals of Kangan and Dalan formations of the South Pars Gas Field were collected for Rock-Eval pyrolysis and measuring TOC content. In the Rock-Eval pyrolysis method during a programmed temperature heating (in a pyrolysis oven) in an inert atmosphere (helium) a small sample (100 mg) is heated. In this experiment, geochemical parameter of the rock, from which TOC is extracted, is determined, quantitatively. The dataset were divided into 8 7 training sets to build the intelligent models, and 37 testing sets to evaluate the reliability of the models.

In the fuzzy inference model, searching for the optimal clustering radius was done by performing clustering process several times and gradually increasing the clustering radius from 0 to 1 (with 0.1 intervals). Thus, several fuzzy models with different number of if-then rules were established. Then, the fuzzy model with the highest overall accuracy was selected as the optimal model for rock type estimation problem.

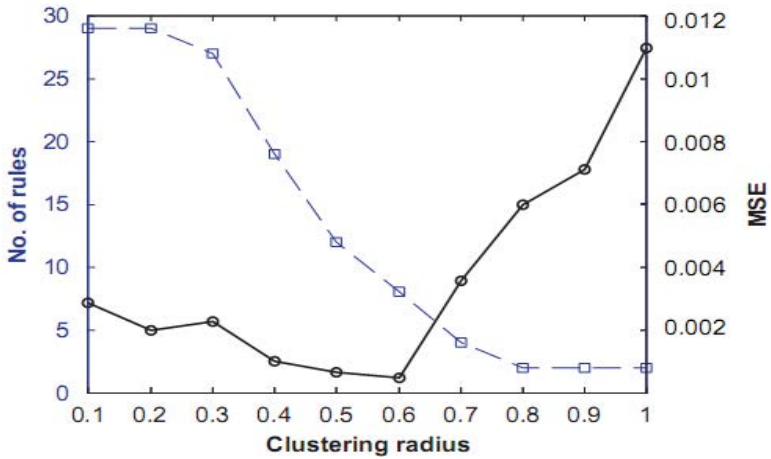

Figure 2.18: Graphs showing clustering radius versus number of generated fuzzy *if–then* rules (dotted blue) and model *MSE* (continuous black). Choosing value of 0.6 is associated with lowest *MSE* resulting in eight fuzzy if–then rules [17].

As shown in figure 2.18 choosing value of 0.6 for clustering radius is associated with the lowest *(MSE)* for the test well and this generates eight fuzzy if–then rules as follows.

1. If (GR is mf4) and (NPHI is mf6) and (DT is mf7) and (RHOB is mf2) and (Rlld is mf5) then (TOC is mf1)

2. If (GR is mf6) and (NPHI is mf8) and (DT is mf6) and (RHOB is mf4) and (Rlld is mf7) then (TOC is mf2)

3. If (GR is mf3) and (NPHI is mf3) and (DT is mf4) and (RHOB is mf5) and (Rlld is mf2) then (TOC is mf3)

4. If (GR is mf2) and (NPHI is mf7) and (DT is mf8) and (RHOB is mf1) and (Rlld is mf3) then (TOC is mf4)

5. If (GR is mf7) and (NPHI is mf1) and (DT is mf1) and (RHOB is mf7) and (Rlld is mf8) then (TOC is mf5)

6. If (GR is mf8) and (NPHI is mf5) and (DT is mf2) and (RHOB is mf8) and (Rlld is mf1) then (TOC is mf6)

7. If (GR is mf5) and (NPHI is mf2) and (DT is mf3) and (RHOB is mf6) and (Rlld is mf6) then (TOC is mf7)

8. If (GR is mf1) and (NPHI is mf4) and (DT is mf5) and (RHOB is mf3) and (Rlld is mf4) then (TOC is mf8)

Thus, the *TS-FIS* model was established by eight membership functions (clusters) for input and output data resulting in eight rules. Input and output membership functions parameters derived by TS-FIS are shown in Table 2.4.

Measured error using *MSE* function is 0.000469 and the R^2 between measured and *FL* predicted TOC is 0.768 (figure 2.19). A comparison between measured and *FL* predicted TOC versus depth in the test data is shown in figure 2.20.

(a)

Inputs	GR (Api)		NPHI (v/v)		DT (μs/ft)		RHOB (gr/cm^3)		Rlld (Ω-m)	
Parameters	σ	μ	σ	μ	σ	μ	σ	μ	σ	μ
Input MF no.										
mf1	2.83	20.84	0.036	0.013	5.93	51.35	0.134	2.04	191.9	54.40
mf2	2.83	21.42	0.036	0.019	5.93	54.41	0.134	2.17	191.9	152.4
mf3	2.83	21.90	0.036	0.091	5.93	59.63	0.134	2.23	191.9	216.7
mf4	2.83	22.47	0.036	0.109	5.93	66.74	0.134	2.25	191.9	260.6
mf5	2.83	23.88	0.036	0.120	5.93	70.89	0.134	2.42	191.9	309.2
mf6	2.83	25.31	0.036	0.134	5.93	73.16	0.134	2.52	191.9	397.9
mf7	2.83	25.78	0.036	0.140	5.93	74.05	0.134	2.61	191.9	621.3
mf8	2.83	30.80	0.036	0.149	5.93	76.57	0.134	2.67	191.9	916.3

(b)

Output	TOC (Wt%)					
	c_1	c_2	c_3	c_4	c_5	c_6
Output MF no.						
mf1	−0.01	31.57	−0.046	−0.22	−0.01	0
mf2	−0.01	−3.18	0.01	−0.27	−0.01	1.30
mf3	−0.04	18.29	0.69	−19.42	0.01	0
mf4	0.20	0	0.029	−2.9	−0.01	0
mf5	0	0	0	0	0.01	0
mf6	0	0	0.01	0	0	0
mf7	0	0	0.11	0	−0.02	0
mf8	−0.29	0	0.34	−14.02	0.01	11.23

Table 2.4: Input (a) and output (b) membership functions parameters derived by TS-FIS.

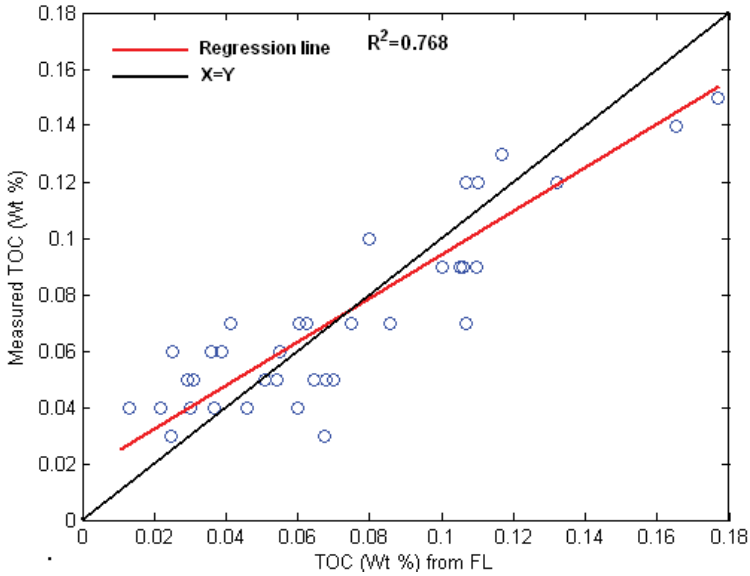

Figure 2.19: Crossplot showing correlation coefficient between measured and *FL* predicted TOC [17].

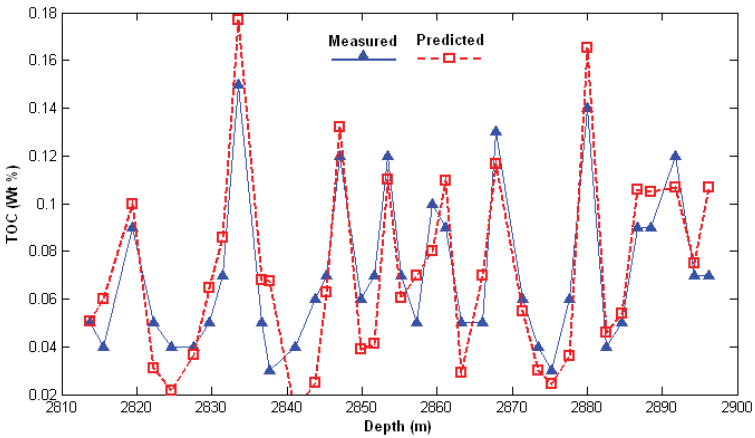

Figure 2.20: A comparison between measured and *FL* predicted *TOC* versus depth in test data [17].

Estimation of Water Saturation from Seismic Attributes

Kadkhodaie et al. (2009b) [18] presented an intelligent model based on fuzzy systems for making a quantitative formulation between 3D seismic attributes and water saturation. Their results based upon a regression analysis revealed that four seismic attributes including time, average frequency, filter 15/20–25/30 and dominant frequency, as the optimal inputs for predicting water saturation (figure 2.21). Their proposed methodology consists of two major steps. At the first step, water saturation (S_w) was predicted from seismic attributes using fuzzy inference systems including Sugeno (1985) [19-22](SFIS), Mamdani (1976 &1977) (MFIS) and Larsen (1985) (LFIS*)*. At the next step, a Committee Fuzzy Inference System (CFIS) was constructed using a hybrid Genetic Algorithms-Pattern Search (GA-PS) technique. The inputs of *CFIS* model were the outputs and average of the mentioned fuzzy

systems each of them had a weight factor showing its contribution in overall prediction. The weights of the *CFIS* add up to one. The schematic diagram of *CFIS* is shown in figure 2.22.

Their methodology was illustrated using a case study. For this purpose, they used 3D seismic data and petrophysical data of 11 wells of the Iranian Offshore Oilfield (figure 2.23) in Persian Gulf Basin. Seismic data were acquired in 2002 and cover a total area of approximately 242 km^2. Ghar Sandstone is the main reservoir unit over the study area. Seismic data quality is generally good over the entire time range with an absence of strong multiple interference. The seismic data are close to zero phase state at the Ghar level. All of the petrophysical data were reviewed and quality controlled. Sonic and density logs were available for all wells.

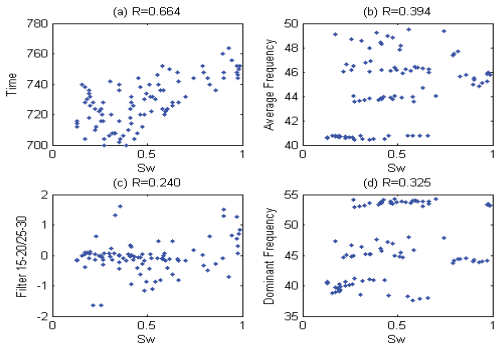

Figure 2.21: Crossplots showing relationships between seismic attributes and water saturation [18].

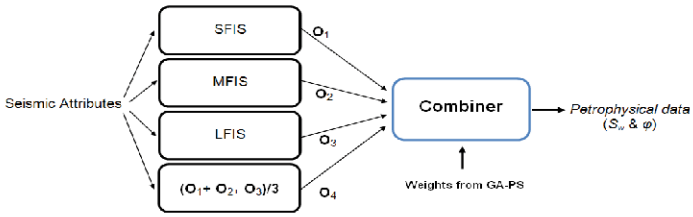

Figure 2.22: A schematic diagram of *CFIS* designed by Kadkhodaie et al. (2009b)[18].

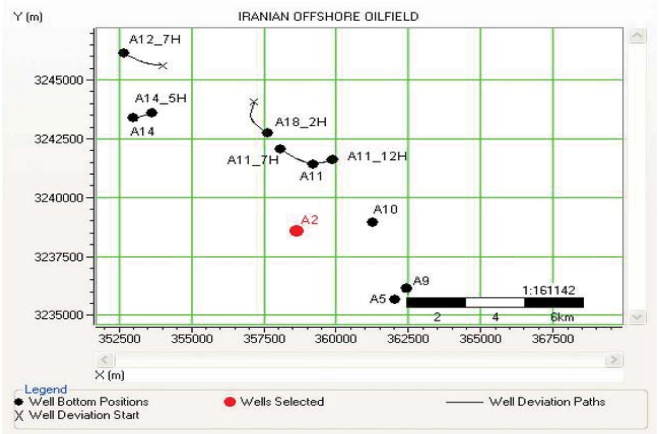

Figure 2.23: Map showing location of wells in Iranian Offshore oilfield [18].

The Fuzzy C-Means Algorithm

The fuzzy c-means algorithm partitions a data set $X = \{x_1,\ldots,x_n\} \subset R^{DIM} = :X$ into c clusters. Each cluster is represented by a prototype $p_k \in R^{DIM}, 1 \le k \le c$. The data- prototype relation is fuzzy, that is, a membership degree $u_{k,j} \in [0; 1]$ indicates the degree of belongingness of data object x_j to prototype p_k or cluster number k. All membership degrees form a membership matrix $U \in R^{c \times n}$. In the classical *FCM* we can interpret the membership degrees as "probabilistic memberships", we have

$$\forall 1 \le j \le n \qquad \sum_{k=1}^{c} u_{k\,j} = 1 \qquad \text{(Eq. 2.7)}$$

The clustering process is carried out by minimizing the objective function

$$J_m = \sum_{j=1}^{n}\sum_{k=1}^{c} (u_{k,j})^m (\|x_j - p_k\|)^2, \qquad \text{(Eq. 2.8)}$$

If the Euclidean distance between datum x_j and prototype p_k is high, J_m is minimized by choosing a low membership degree near 0. If the distance is small, the membership degree approaches 1. J_m is effectively minimized by alternating optimization, that is, we alternatively minimize Eq. (2.8) with respect to the prototypes (assuming memberships to be constant) and then with respect to the membership degrees (assuming prototypes to be constant). In both minimization steps, we obtain closed form solutions, for the prototypes [23]:

$$p_k = \frac{\sum_{j=1}^{n} (u_{k,j})^m x_j}{\sum_{j=1}^{n} (u_{k,j})^m}, \forall 1 \le k \le c \qquad \text{(Eq. 2.9)}$$

And for the membership degrees

$$u_{k,j} = \begin{cases} \dfrac{1}{\sum_{l=1}^{c} \left(\dfrac{|x_j - p_k|^{2(m-1)}}{|x_j - p_k|^{2(m-1)}}\right)} & \text{in case } I_j = 0 \\ \dfrac{1}{|I_j|} & \text{in case } I_j \ne 0, k \in I_j \\ 0 & \text{in case } I_j \ne 0, k \notin I_j \end{cases} \qquad \text{(Eq. 2.10)}$$

The FCM algorithm is as follows

1. choose fuzzifier m > 1;
2. choose termination threshold ε > 0;
3. initialize prototypes p_k;
4. **repeat**
5. update memberships using (4);
6. update prototypes using (3);
7. **until** change in memberships drops below ε;

For the sake of simplicity, let us assume that it will never happen that a prototype matches a data object perfectly, or in other words the Euclidean distance between any pair of data object and prototype never vanishes. Then, we have no need for considering special cases as in (4), I_j is always empty. In practice, we can add a small constant η>0 near the floating point precision to all distance values to guarantee this. We reformulate the membership degrees between data objects and prototypes as a function (Eq. 2.11);

Where q=2/ (m-1) and $P := \left(R^{DIM}\right)^c$. If **p** denotes the tuple of prototypes (p_1,..., p_c) then we have $u_{k,j} = u_k (x_j ; \mathbf{p})$.

Fuzzy Model Descriptions

In order to construction of MFIS and LFIS for estimating S_w, fuzzy rule base was generated through FCM derived input and output cluster centres. Each cluster centre was used to generate a Gaussian membership function in each rule. That is, each rule is represented by a Gaussian MF which is constructed from centre and standard deviation of corresponding cluster. So, number of membership functions and if-then rules for each input and output dataset is equal to number of the clusters. As mentioned, number of the FCM derived clusters for water saturation was equal to 31. Considering four inputs and one output, 31 by 5 MFs were generated participating in 31 fuzzy rules (Table 2.5). To connect antecedents of each rule min operator was used. As mentioned, fuzzy rule base structure for MFIS and LFIS is similar. Their main difference is in implication method. In MFIS, min operator was used for implication, whereas in LFIS product operator was used for this purpose. For the both techniques, centroid defuzzification method was applied.

In SFIS, input MFs are of Gaussian type. They were constructed using the cluster centres obtained from subtractive clustering (43 clusters for S_w). But, output membership functions are linear equations constructed from inputs. For example, output MF1 of S_w model, which is the consequent of rule no. 1, is constructed from four seismic attributes as below:

Output MF1=

γ_1*Time + γ_2*Average frequency + γ_3*Filter15/20-25/30 + γ_4*Dominant frequency + γ_5 (Eq. 2.12)

In this equation, parameters γ_1, γ_2, γ_3 and γ_4 are coefficients corresponding to input seismic attributes. Parameter γ_5 is the constant of each equation. These parameters are obtained by linear least squares estimation. With these explanations in order to estimate S_w there will be 43 by 5 output MF parameters (Table 2.6).

Construction of CFIS

In this part of research, a CFIS was constructed for the overall prediction of petrophysical data by integrating the results of predicted data from SFIS, MFIS \and LFIS each of them has a weight factor showing its contribution in overall prediction. At the first step, outputs of the three fuzzy inference systems were averaged for predicting target data, namely each of them has the weight value of 0.333. This output will be used as one of the experts of the CFIS.

In the next step, a genetic algorithm-pattern search tool was used to obtain optimal combination of the weights for constructing CFIS. The fitness function for GA-PS was defined as below:

Rule No.	MF No.	Time		Average frequency		Filter 15/20-25/30		Dominant frequency		Water saturation	
		σ	Mean	σ	Mean	σ	Mean	Σ	Mean	σ	Mean
1	MF1	8.096	759.000	0.487	44.990	0.154	0.082	1.393	43.970	0.068	0.952
2	MF2	5.506	746.200	0.513	45.410	0.411	1.404	1.459	44.290	0.072	0.949
3	MF3	4.222	734.200	0.542	45.830	0.237	-0.643	1.498	44.590	0.059	0.837
4	MF4	7.026	701.300	1.039	40.430	0.139	0.033	1.811	41.090	0.048	0.566
5	MF5	4.051	731.900	0.573	45.530	0.250	-0.685	1.915	53.900	0.048	0.713
6	MF6	4.972	712.000	0.589	43.760	0.144	0.027	1.839	53.430	0.058	0.664
7	MF7	6.262	704.700	0.756	46.870	0.448	1.548	1.410	45.250	0.044	0.594
8	MF8	5.349	745.500	1.013	40.760	0.142	-0.088	2.494	38.280	0.046	0.722
9	MF9	4.577	738.100	0.549	46.070	0.227	-0.606	1.844	53.590	0.046	0.673
10	MF10	6.060	705.700	0.590	43.630	0.143	0.066	1.774	53.070	0.051	0.543
11	MF11	6.222	750.400	0.504	45.270	0.392	1.355	1.439	44.180	0.075	0.971
12	MF12	3.835	724.200	1.058	40.680	0.150	0.030	2.174	39.960	0.068	0.471
13	MF13	3.869	723.800	0.608	46.180	0.470	-1.595	1.514	44.820	0.060	0.520
14	MF14	3.886	727.500	0.594	44.930	0.197	-0.391	1.943	54.010	0.049	0.668
15	MF15	3.972	730.400	0.561	45.960	0.388	-1.306	1.507	44.680	0.048	0.624
16	MF16	6.214	750.600	0.997	40.760	0.140	-0.106	2.575	37.780	0.047	0.778
17	MF17	4.057	719.900	0.644	46.310	0.347	-1.112	1.508	44.910	0.049	0.678
18	MF18	3.869	727.600	0.578	46.050	0.470	-1.616	1.512	44.740	0.070	0.471
19	MF19	4.903	712.300	1.055	40.580	0.145	-0.166	1.977	40.640	0.091	0.378
20	MF20	4.194	718.200	1.059	40.640	0.143	-0.097	2.075	40.320	0.075	0.442
21	MF21	4.563	738.100	0.529	45.700	0.185	0.204	1.487	44.490	0.069	0.917
22	MF22	5.254	744.300	0.523	45.940	0.164	0.098	1.808	53.420	0.077	0.954
23	MF23	6.213	750.300	0.503	45.810	0.254	0.719	1.770	53.230	0.079	0.991
24	MF24	4.221	718.400	0.596	44.050	0.145	-0.029	1.890	53.760	0.045	0.652
25	MF25	5.548	708.300	0.733	46.730	0.385	1.254	1.437	45.170	0.048	0.569
26	MF26	5.862	706.600	1.047	40.510	0.139	-0.107	1.888	40.890	0.046	0.592
27	MF27	4.429	716.000	0.684	46.450	0.175	-0.303	1.492	45.000	0.059	0.523
28	MF28	4.939	712.100	0.708	46.590	0.246	0.577	1.464	45.080	0.063	0.487
29	MF29	3.922	722.900	0.592	45.420	0.162	-0.208	1.922	53.940	0.049	0.759
30	MF30	7.131	754.800	0.495	45.130	0.274	0.836	1.415	44.070	0.074	0.976
31	MF31	4.977	742.100	0.520	45.560	0.319	0.969	1.475	44.390	0.070	0.930

Table 2.5: Gaussian membership function parameters derived by FCM for predicting Sw (Kadkhodaie et al., 2009b)[18].

$$MSE_{CMIS} = \sum_{i=1}^{l} 1/k(\beta_1 O_{1i} + \beta_2 O_{2i} + \beta_3 O_{3i} + \beta_4 O_{4i} - L_i)^2 \qquad \text{(Eq. 10)}$$

This function shows the MSE of CFIS for training step predictions where β_1 , β_2, β_3 and β_4 are the weight coefficients corresponding to the outputs of Sugeno, Mamdani, Larsen and simple averaging method, respectively. O_i and L_i are output and target values, respectively. k is the number of test data (76 samples). Parameters of GA-PS are described as following:

Population is of a double vector type. Initial population size is 25 which specifies how many individuals are in each generations. Initial range is [0, 1]. This parameter specifies the range of the vectors in the initial population. The selection function was chosen as stochastic uniform which chooses parents for the next generation based on their scaled values from the fitness scaling function. The crossover function is scattered that creates a random binary vector and selects the genes where the vector is [1] from the first parent, and the genes where the vector is [0] from the second parent, and combines the genes to form a child. The value of crossover fraction is 0.78. This parameter specifies the fraction of the population that could be seen in the crossover children. Mutation function is Gaussian that adds a random number, or mutation, from a Gaussian distribution, to each entry of the parent vector. Parameters controlling the mutation are specified as the scale value of 1 and shrink value of 1. The scale value controls the standard deviation of the mutation at the first generation. This parameter is multiplied by the range of the initial population. Shrink value controls the rate at which the average amount of mutation decreases. The standard deviation decreases linearly so that its final value equals 1. Hybrid function was chosen as pattern search. This is another minimization function that runs after genetic algorithm terminates.

Stopping generation of GA was chosen as 100. After 100 generations, change in the fitness function values over Stall generations was insignificant and the mean fitness value for water saturation was fixed in 0.00915. Finally, CFIS was constructed using the GA-PS

derived coefficients for the results of SFIS, MFIS, LFIS and simple averaging method. Final estimation of water saturation was done through Eq. (2.13).

$$Sw_{CFIS} = 0.303 * Sw_{SFIS} + 0.127 * Sw_{MFIS} + 0.098 * Sw_{LFIS} + 0.472 * Sw_{Average} \quad \text{(Eq. 2.13)}$$

Rule No.	MF No.	Time		Average frequency		Filter 15/20-25/30		Dominant frequency		Water saturation				
		σ	Mean	σ	Mean	σ	Mean	σ	Mean	γ_1	γ_2	γ_3	γ_4	γ_5
1	MF1	3.182	732	0.481	40.720	0.095	0.107	0.883	39.400	0.008	0.000	0.000	-0.131	0.000
2	MF2	3.182	716	0.481	40.610	0.095	-0.140	0.883	40.430	0.017	0.000	0.000	-0.294	0.000
3	MF3	3.182	724	0.481	48.440	0.095	0.335	0.883	46.070	-0.001	0.000	0.000	0.027	0.000
4	MF4	3.182	720	0.481	40.640	0.095	-0.060	0.883	40.200	0.001	0.000	0.000	0.000	0.000
5	MF5	3.182	708	0.481	43.680	0.095	0.053	0.883	53.220	0.001	0.000	0.000	0.000	0.000
6	MF6	3.182	752	0.481	40.750	0.095	-0.103	0.883	37.640	0.001	0.000	0.000	0.000	0.000
7	MF7	3.182	708	0.481	48.980	0.095	-0.424	0.883	47.140	0.001	0.000	0.000	0.000	0.000
8	MF8	3.182	740	0.481	40.750	0.095	-0.004	0.883	38.760	-0.005	0.000	0.000	0.097	0.000
9	MF9	3.182	748	0.481	47.510	0.095	-0.321	0.883	44.100	0.001	0.000	0.000	0.000	0.000
10	MF10	3.182	720	0.481	43.900	0.095	-0.056	0.883	53.840	0.001	0.000	0.000	0.000	0.000
11	MF11	3.182	736	0.481	46.110	0.095	-0.810	0.883	53.660	0.001	0.000	0.000	0.000	0.000
12	MF12	3.182	704	0.481	40.470	0.095	-0.049	0.883	40.990	0.001	0.000	0.000	0.000	0.000
13	MF13	3.182	716	0.481	48.720	0.095	-0.018	0.883	46.630	0.001	0.000	0.000	0.000	0.000
14	MF14	3.182	732	0.481	44.060	0.095	-0.173	0.883	54.290	0.002	0.000	0.000	0.000	0.000
15	MF15	3.182	748	0.481	45.860	0.095	0.541	0.883	53.320	0.001	0.000	0.000	0.000	0.000
16	MF16	3.182	732	0.481	48.140	0.095	0.045	0.883	45.470	0.001	0.000	0.000	0.000	0.000
17	MF17	3.182	724	0.481	46.340	0.095	-0.426	0.883	53.910	0.001	0.000	0.000	0.000	0.000
18	MF18	3.182	740	0.481	47.840	0.095	-0.452	0.883	44.810	0.001	0.000	0.000	0.000	0.000
19	MF19	3.182	692	0.481	49.480	0.095	0.477	0.883	48.000	0.001	0.000	0.000	0.000	0.000
20	MF20	3.182	740	0.481	46.030	0.095	-0.435	0.883	53.550	0.001	0.000	0.000	0.000	0.000
21	MF21	3.182	704	0.481	49.110	0.095	-0.388	0.883	47.370	0.000	0.000	0.000	0.000	0.000
22	MF22	3.182	728	0.481	44.010	0.095	-0.158	0.883	54.160	0.000	0.000	0.000	0.000	0.000
23	MF23	3.182	720	0.481	46.410	0.095	0.071	0.883	53.980	0.001	0.000	0.000	0.000	0.000
24	MF24	3.182	744	0.481	45.950	0.095	0.066	0.883	53.440	0.001	0.000	0.000	0.000	0.000
25	MF25	3.182	696	0.481	49.360	0.095	0.170	0.883	47.800	0.001	0.000	0.000	0.000	0.000
26	MF26	3.182	700	0.481	40.410	0.095	0.073	0.883	41.140	0.001	0.000	0.000	0.000	0.000
27	MF27	3.182	736	0.481	47.990	0.095	-0.237	0.883	45.140	0.001	0.000	0.000	0.000	0.000
28	MF28	3.182	700	0.481	49.240	0.095	-0.163	0.883	47.590	0.001	0.000	0.000	0.000	0.000
29	MF29	3.182	752	0.481	47.350	0.095	0.026	0.883	43.730	0.001	0.000	0.000	0.000	0.000
30	MF30	3.182	732	0.481	46.190	0.095	-0.946	0.883	53.750	0.001	0.000	0.000	0.000	0.000
31	MF31	3.182	744	0.481	40.750	0.095	-0.075	0.883	38.410	0.001	0.000	0.000	0.000	0.000
32	MF32	3.182	752	0.481	45.770	0.095	0.849	0.883	53.190	0.001	0.000	0.000	0.000	0.000
33	MF33	3.182	728	0.481	46.260	0.095	-0.803	0.883	53.830	0.001	0.000	0.000	0.000	0.000
34	MF34	3.182	708	0.481	40.520	0.095	-0.142	0.883	40.830	0.001	0.000	0.000	0.000	0.000
35	MF35	3.182	712	0.481	43.760	0.095	0.028	0.883	53.450	0.001	0.000	0.000	0.000	0.000
36	MF36	3.182	724	0.481	43.960	0.095	-0.111	0.883	54.010	0.002	0.000	0.000	0.000	0.000
37	MF37	3.182	720	0.481	48.580	0.095	0.222	0.883	46.360	0.001	0.000	0.000	0.000	0.000
38	MF38	3.182	744	0.481	47.680	0.095	-0.494	0.883	44.460	0.001	0.000	0.000	0.000	0.000
39	MF39	3.182	712	0.481	48.850	0.095	-0.274	0.883	46.890	0.001	0.000	0.000	0.000	0.000
40	MF40	3.182	716	0.481	43.830	0.095	-0.008	0.883	53.660	0.001	0.000	0.000	0.000	0.000
41	MF41	3.182	748	0.481	40.750	0.095	-0.115	0.883	38.030	0.001	0.000	0.000	0.000	0.000
42	MF42	3.182	704	0.481	43.600	0.095	0.075	0.883	52.970	0.001	0.000	0.000	0.000	0.000
43	MF43	3.182	724	0.481	40.670	0.095	0.031	0.883	39.960	0.001	0.000	0.000	0.000	0.000

Table 2.6: Gaussian and linear membership function parameters derived by subtractive clustering and gradient descent methods for predicting Sw using SFIS [18].

Performance of the *CFIS* model was compared to that of a Probabilistic Neural Network *(PNN)*. The results (figure 2.24) show that *CFIS* method performs better than neural network, best individual fuzzy model and simple averaging method.

Using the methodology of *CFIS*, 3D cube of seismic data and their attributes were converted to water saturation volume. A map water saturation distribution estimated from *CFIS* model is shown in figure 2.25. As shown, water saturation in the central and North West sector of the reservoir is low (< 50%), which corresponds to the hydrocarbon-bearing area.

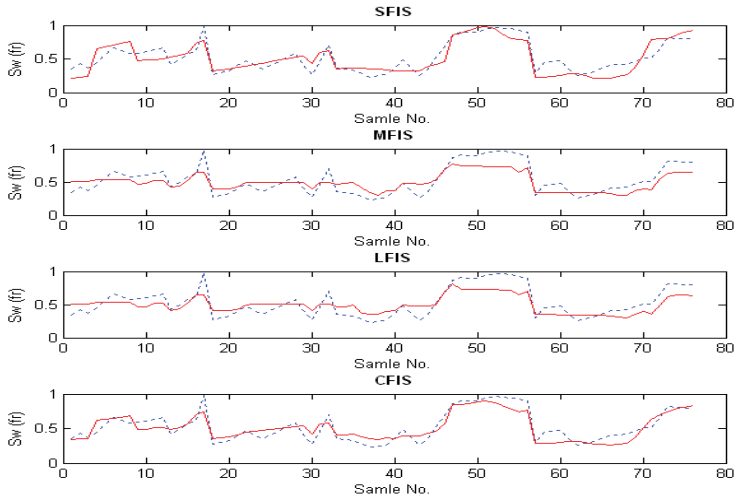

Figure 2.24: Graphical comparison between measured and predicted water saturation for test samples using *SFIS* (a), MFIS (b), *LFIS* (c) and *CFIS* (d) [18].

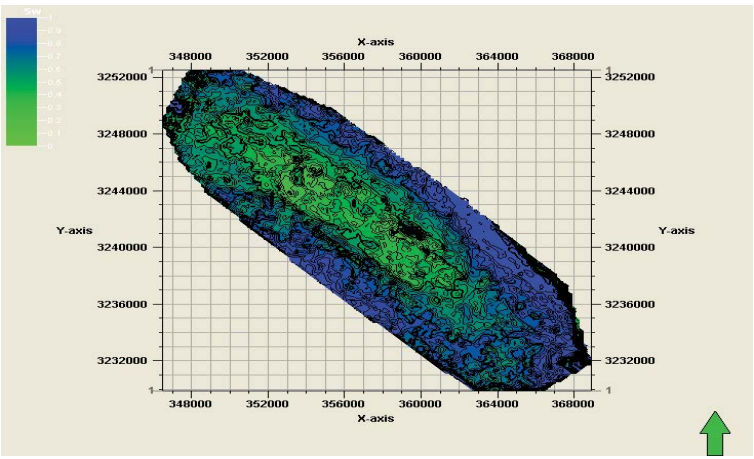

Figure 2.25: Map showing distribution of *CFIS* estimated water saturation for Top Ghar reservoir [18].

Rock Types Classification and Estimation

Lithofacies typing is useful in well correlation and can be important for building a 3D model of the field by geostatistical or stochastic techniques. These models can be used for volumetrics, well placing and reservoir engineering. Using fuzzy logic for lithofacies prediction makes no assumptions and retains the possibility that a particular facies type can give any log reading although some are more likely than others. This error or fuzziness has been measured and used to improve the facies prediction.

The Iran offshore gas field, the Iranian part of the world's largest non-associated gas accumulation is located in the Persian Gulf between Qatar and Iran, some 100 km from shore. The Upper Permian to Lower Triassic Dalan and Kangan Formations are two huge, condensate rich and gas bearing reservoirs over the field. In a case study from the Iranian offshore gas field by Kadkhodaie et al. (2006)[9], reservoir rock types were determined based on core porosity and permeability data and a fuzzy centre means clustering *(FCM)*. Then, the *FCM* clustering derived rock types were estimated from well log data using fuzzy mathematics. Gaussian function was used to estimate relative probability or "fuzzy possibility" that a data value belongs to each rock type. Each log data value may belong to any of *FCM* clustering derived rock types to a degree that can be calculated from Gaussian membership function using Eq. (2.14).

$$P(x) = \frac{e^{-\frac{1}{2}(x-c)^2/(\sigma)_2}}{(\sigma)\sqrt{2\pi}} \qquad \text{(Eq. 2.14)}$$

Each rock type has its own mean and standard deviation, namely, for n number of rock types; there are n pairs of c and σ rock type. For example, the fuzzy possibility that a neutron log data belongs to rock type 1 is obtained by substituting $\sigma_{rock\ \ type1}$ and $\sigma_{rock\ \ type1}$ in Eq. (2.15):

$$P(N) = \frac{e^{-(NPHI-C_{rock\ \ type1})^2/(\sigma_{rock\ \ type1})_2}}{(\sigma_{rock\ \ type1})\sqrt{2\pi}} \qquad \text{(Eq. 2.15)}$$

The ratio of the fuzzy possibility for each rock type with the fuzzy possibility of the mean or most likely observation is obtained by de-normalizing Eq. (2.16). The fuzzy possibility for mean of neutron in rock type 1 is obtained by substituting NPHI by $c_{rock\ \ type1}$ in Eq. (2.16):

$$P(c_{rock\ \ type1}) = \frac{e^{-(C_{rock\ \ type1}-C_{rock\ \ type1})^2/(\sigma_{rock\ \ type1})_2}}{(\sigma_{rock\ \ type1})\sqrt{2\pi}} \qquad \text{(Eq. 2.16)}$$

The relative fuzzy possibility $R(N_{rock\ type\ 1})$ of a neutron porosity (NPHI) belonging to rock type 1 compared to the fuzzy possibility of measuring the mean value $c_{rock\ \ type1}$ is Eq. (2.15) divided by Eq. (2.16):

$$R(N_{RT1}) = e^{-(NPHI-C_{rock\ \ type1})^2/(\sigma_{rock\ \ type1})_2} \qquad \text{(Eq. 2.17)}$$

Each value derived from Eq. (2.17) is now indicated to possible rock types. To compare the relative fuzzy possibilities of this equation among rock types, Eq. (2.17) is multiplied by a coefficient named relative occurrence of each rock type in the reservoir interval. For rock type 1, it is notified by $\sqrt{n_{rock\ \ type1}}$:

$$F(NPHI_{rock\ \ type1}) = (\sqrt{n_{rock\ \ type1}})e^{-(NPHI-C_{rock\ \ type1})^2/(\sigma_{rock\ \ type1})_2} \qquad \text{(Eq. 2.18)}$$

The obtained fuzzy possibility from Eq. (2.18) is based on neutron log data only. This process should be repeated for other logs such as sonic (DT), density (RHOB), ... at this point. This will give F*(DTrock type1)*, *F(RHOBrock type1)*, ... for rock type 1. These fuzzy possibilities are combined harmonically to give a final fuzzy possibility:

$$\frac{1}{C_{rock\ \ type1}} = \frac{1}{F(NPHI_{rock\ \ type1})} + \frac{1}{F(DT_{rock\ \ type1})} \qquad \text{(Eq. 2.19)}$$

This process is repeated for other rock types and all derived fuzzy possibilities are combined harmonically. Then, the rock type with the highest combined fuzzy possibility is taken as most possible rock type at that point. A comparison between *FCM* clustering derived and fuzzy predicted rock types versus depth for the test well that was not used to model construction (the test well) is shown in figure 2.26.

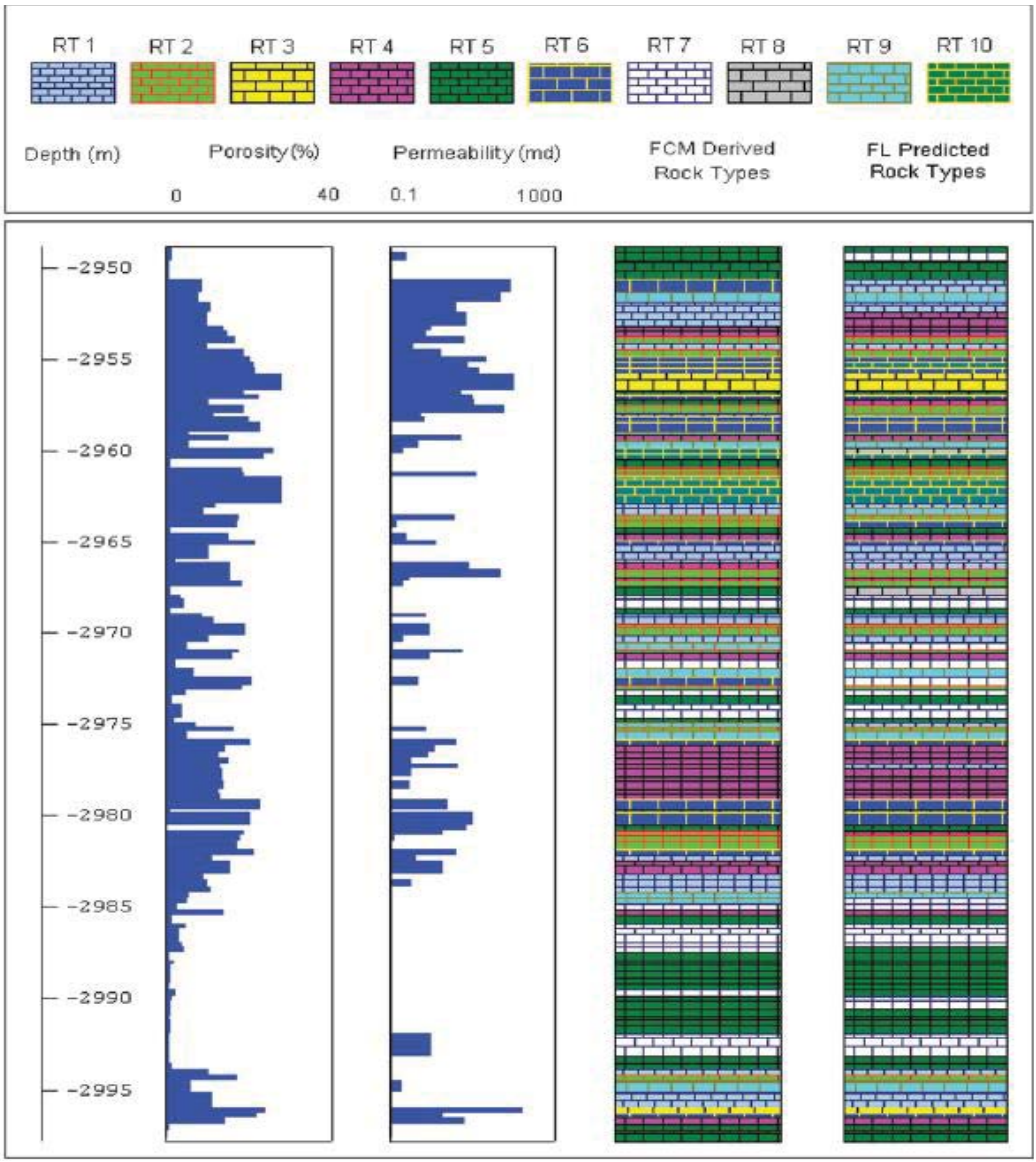

Figure 2.26: A comparison between clustering derived and fuzzy predicted rock types versus depth for the test well in Kangan Formation, Iranian offshore gas field [9].

In a similar study from the Southern North Sea, Cuddy (1998)[1] studied the lithofacies estimation using the fuzzy logic model in the Permian Rotliegendes Sandstone (Viking). The Viking field was developed in 1972 and to date has produced 2.8 Tcf of gas. Consideration has recently been given to tying back several smaller satellite pools. As part of the feasibility study, 13 exploration and production wells, drilled between 1969 and 1994, have been re-evaluated using fuzzy logic.

The reservoir was deposited in a desert by aeolian, fluvial, and lacustrine processes. Three major lithofacies associations have been recognised from core studies:

Aeolian Dune: Aeolian sandstones have the best permeability by virtue of their better sorting and lack of detrital clays. Clean aeolian dune sandstones give the highest porosities in the reservoir, with an average around 16 pu. Dune base sandstones (wind ripple) give a lower average porosity of 12-14 pu, as they are less well sorted.Sabkha: Sandy sabkha has good porosity but the presence of detrital clay enhances compaction effects and thus reduces primary porosity. Muddy sabkha porosities and permeability are very low with no reservoir potential. Fluvial: The fluvial sandstones often have poorer permeabilities (<0.3 mD) and porosities (<10 pu) than the sandy sabkha sandstones. Their porosity is dependent on the detrital clay content and pore filling cements.

In addition, in all lithofacies, diagenetic overprint of pervasive fibrous illite clays severely reduces permeabilities. Only in the well-sorted grain-flow lithofacies that has a macro-porous network are moderate permeabilities retained. The object of applying fuzzy logic to this field was to differentiate lithofacies types in uncored wells and to help with building the reservoir model of the field and with future well placing.

One recent well with substantial core coverage was used to calibrate lithofacies and permeability predictor for the older wells. The left track of figure 2.27 shows the core described facies from this well. There are several lithofacies described, aeolian, fluvial and sabkha. The aeolian is sub-divided into grainflow, wind-ripple and sand sheet, the sabkha into sandy, mixed and muddy and the fluvial into cross-bedded and structure-less. The result of the fuzzy predicted lithofacies is shown in the second track. There is near perfect differentiation between aeolian, fluvial and sabkha rock types. In addition, the technique goes some way towards differentiating between sandy, mixed and muddy sabkhas. The right track shows the comparison of core derived and fuzzy predicted permeabilities. It must be remembered that the core descriptions themselves are from observations and can contain errors due to the subjective nature of the measurement. Consequently, predicted lithofacies can be used by sedimentologists as an aid to refining core interpretations. This example of a self-calibrated well has helped the sub-surface team develop the Viking satellites. “Blind-testing” between wells can test the predictive ability of the technique in the same field. This was conducted on data from the South Ravenspurn field.

South Ravenspurn gas field is located in the Southern North Sea, 40 miles off the English coast. Reserves are around 1 Tcf and current production is 200 mmscf/d. The field is developed by some 40 wells in shallow water no more than 50 meters deep. Descriptions from 10 cored wells were used to derive facies in 30 uncored wells. The left well shown in figure 2.28 shows the described and predicted facies types for one cored well in the field. The prediction success rate is over 86% compared to a random prediction rate of 13%. The prediction success rate is calculated as the number of correct predictions divided by the total number of possible predictions.

Using the fuzzy relationships between the described lithofacies and electrical logs, lithofacies were predicted in a second well shown on the right of figure 2.28. The prediction success in this second well between the predicted facies and “hidden” described facies is 73%, with the majority of the “failed” predictions falling into the next closest lithofacies type rather than one with completely different reservoir characteristics.

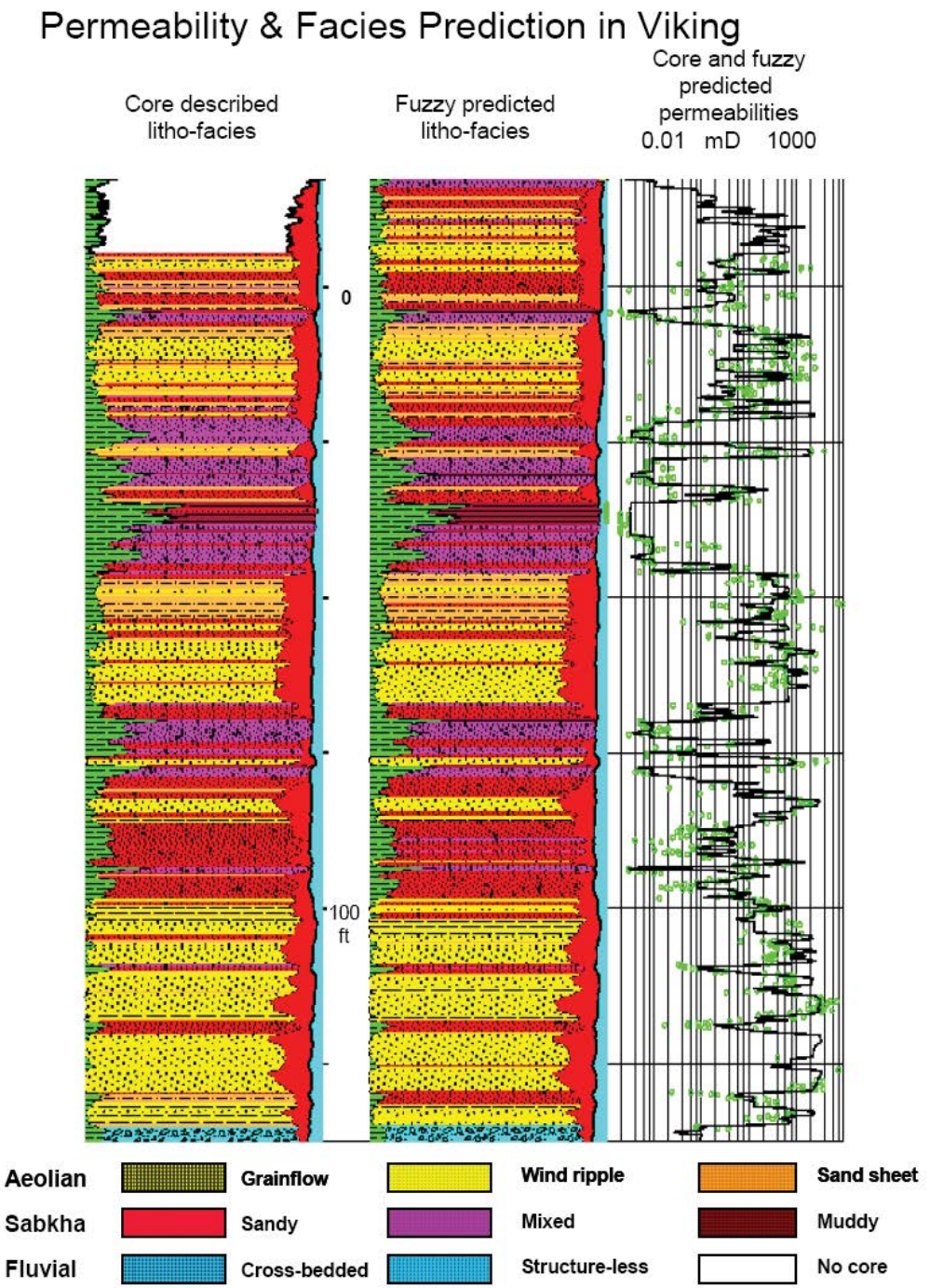

Figure 2.27: Core described facies from training well [1].

Figure 2.28: The described and predicted facies types for one cored well in the field [1].

Rock Recognition from Drilling Sensor Data

As shown by (Kadkhodaie et al., 2010)[24] Measurement while drilling (MWD) data could be considered as important input data for rock recognition. *MWD* sensors such as bit pressure, rotation pressure, pull-down pressure, pull-down rate, head speed and pressure transducers can tell us information regarding rock types being drilled. The *MWD* sensors used for the rock recognition were bit air pressure, pull-down pressure, rotation pressure, pull-down rate, head speed and seven pressure transducers including feed down, feed up, reverse rotation, forward rotation, rotation relief, feed relief and hold back from 28 blast holes in a Western Australia's iron ore mine (figure 2.29) for the study of rock recognition. The above mentioned input data of drill sensors were chosen based upon the fact they are strongly correlated to lithology of drilled rock. Actually, when there are many inputs available there many methods to choose the optimal set of input data whose details can be found in works of Zoveidavianpoor et al. (2012) and Zoveidavianpoor et al. (2014)[25,26]. The study site is chosen because a variety of down-hole conditions were expected to vary. Three rows of holes are drilled with the drill operating in percussion mode (down-hole hammer) with and without shock absorber, and rotary mode with and without shock absorber. Of the three rows of holes, row 1 is the most comprehensive. In this row, 28 holes 12 m deep are drilled at 3 m spacings with the drill in percussion mode and with the use of the shock absorber. At the completion of the drilling all blast holes are geophysical logged using caliper, natural gamma, magnetic susceptibility and density logging tools. The detailed geology is determined by site geologists using a combination of core logging and the geophysical logging results. A geological section through the holes 1 to 28 is shown in figure 2.30. As shown, the holes intersected a number of rock types including *shale*, *iron ore* and Banded Iron Formation (BIF).

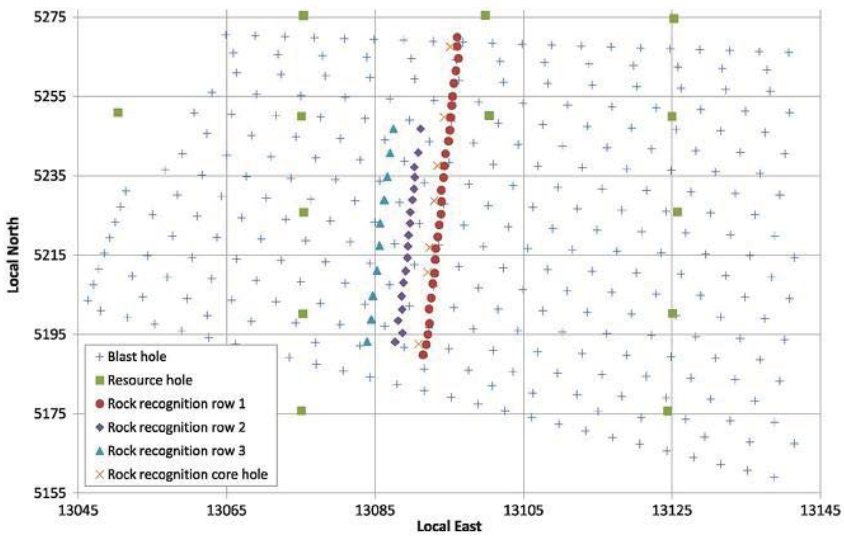

Figure 2.29: Map showing location of (brown round dots) the blast holes in the study area.

In this study, fuzzy inference system is used for supervised learning of classifiers. Let $\{\boldsymbol{x}_i, \boldsymbol{Y}_i\}_{i=1}^{N}$ be a set of N training samples. Each sample is a pair of sequences $(\boldsymbol{x}_i, \boldsymbol{Y}_i)$, where $\boldsymbol{x}_i = \{x_{i,1}, x_{i,2}, \ldots, x_{i,T_i}\}$ and $\boldsymbol{Y}_i = \{Class_{i,1}, Class_{i,2}, \ldots, Class_{i,T_i}\}$. The goal is to construct a classifier m that can correctly predict a new label sequence $Y = m(x)$ given an input sequence $\boldsymbol{x}$. Here, the output classes are rock labels and inputs are drilling sensor data.

The optimal number of membership functions and their parameters was extracted by a subtractive clustering process. Searching for the optimal clustering radius was done by

performing clustering process several times and gradually increasing the clustering radius from 0.005 to 1 (with 0.005 intervals). Thus, 200 fuzzy models with different number of if-then rules were established. Then, the fuzzy model with the highest overall accuracy was selected as the optimal model for rock type estimation problem. The accuracy, precision and recall of the fuzzy models versus clustering radius are shown in figure 2.32. As shown, choosing the value of 0.155 for the clustering radius is associated with the highest accuracy (74.1%) and this generates 13 fuzzy clusters for each of the 12 input drilling data. Thus, the TS-FIS model was established by a matrix of 12 by 13 membership functions (clusters) resulting in 156 fuzzy rules. Generated fuzzy if-then rules are shown in figure 2.31, graphically.

The results show the accuracy of 74.1 % between ground truth and predicted rock types for 28 blast holes using fuzzy logic (figure 2.33).The analysis of MWD parameters fuzzy systems indicates that the mechanical measurements produce a response corresponding to changes in rock strength which can reveal changes in lithology. For example, the strength of the BIF is greater than for the iron ore zone which in turn is greater than for the shales. It is also important to understand the relationship between a set of inputs and the resulting outputs of the fuzzy model.

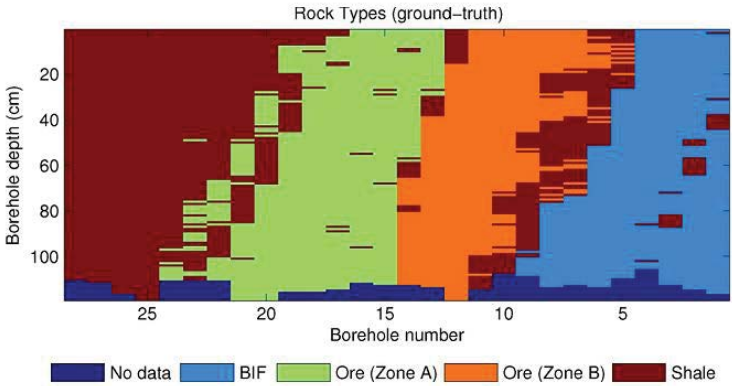

Figure 2.30: A geological section through holes 1 to 28 used for training models (Kadkhodaie et al., 2010).[24].

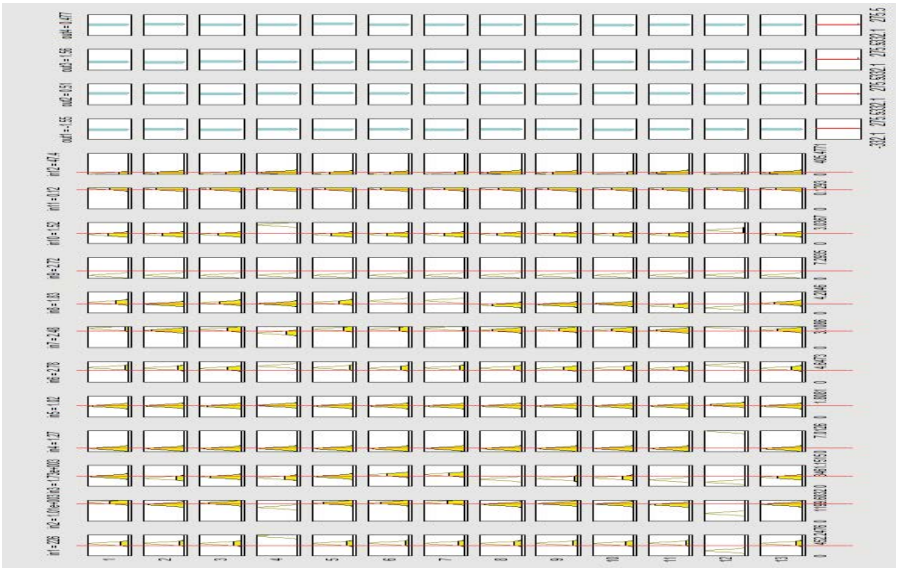

Figure 2.31: Graphical illustration showing TS-FIS model by a matrix of 12 by 13 membership functions.

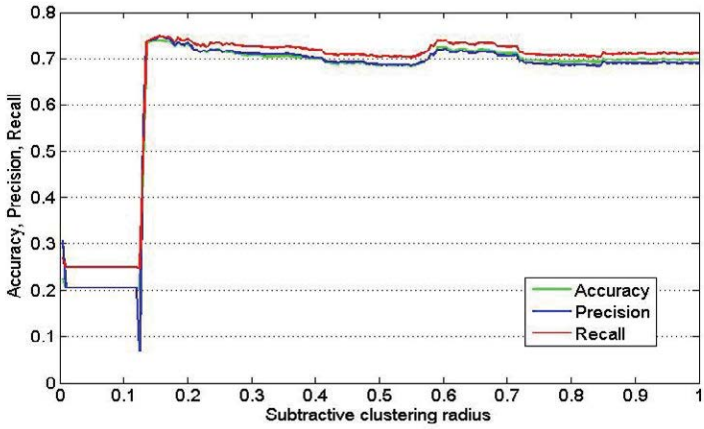

Figure 2.32.: Accuracy, recall and precision versus clustering radius, optimizing fuzzy model parameter [24].

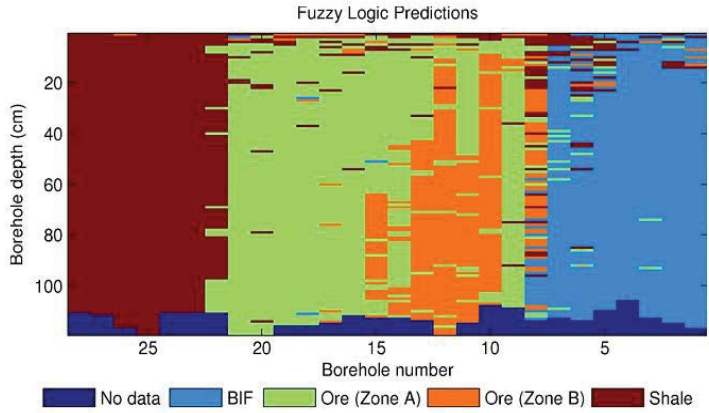

Figure 2.33: Estimated rock types for 28 blast holes using fuzzy logic [24].

Conclusion

In this chapter, application of fuzzy inference systems to extraction of hidden rock properties in the geological, petrophysical, seismic and drilling sensor data (MWD) was studied. Rock properties estimation using fuzzy models provides very useful information for reservoir characterization and development. It is shown that fuzzy models can successfully be applied to the estimation of porosity, permeability, water saturation, shear wave velocity, total organic carbon, nuclear magnetic resonance log, conventional logs (neutron, sonic, density and resistivity), lithology and rock types. Fuzzy logic can reduce uncertainty in reservoir data analysis and will aid in successful implementation of the master development plans. It is hoped that a fuzzy inference system that can easily accommodate new information will be a comprehensive model. The main requirement will be for a training set consisting of input data and corresponding output data. This will allow extreme flexibility for using the method with different reservoir data types and different geological conditions.

References

1. Cuddy SJ (1998) Litho-facies and Permeability Prediction from Electrical Logs using Fuzzy Logic, SPE 65411 (49470), 8th Abu Dhabi International Petroleum Exhibition and Conference.
2. Walpole F (1980)Mathematical Statistics. Prentice / Hall International. 206 P.
3. Nikolaidis, E (2005) Types of uncertainty in design decision making. In: Nikolaidis E, Ghiocel DM, Singhal S (eds) Engineering design reliability handbook. CRC Press, New York.
4. Zoveidavianpoor M, Gharibi M, 2015. Applications of Type-2 Fuzzy Logic System: Handling the Uncertainty Associated with Candidate-well Selection for Hydraulic Fracturing, Neural Computing & Application. In press. doi:10.1007/s00521-015-1977-x, Pp. 1-21.
5. Rezaee MR, Kadkhodaie-Ilkhchi A and Barabadi A, (2007) Prediction of shear wave velocity from petrophysical data utilizing intelligent systems: an example from a sandstone reservoir of Carnarvon Basin, Australia. Journal of Petroleum Science and Engineering, 55, 201-212.
6. Rezaee MR, Kadkhodaie, A., 2008. Intelligent approach for the synthesis of petrophysical logs. Journal of Geophysics and Engineering, UK, Vol. 5, pp 12-26.
7. Chiu, S., 1994. Fuzzy model identification based on cluster estimation. Journal of Intelligent and Fuzzy Systems 2, 267-278.
8. Rezaee MR, Slatt R, Kadkhodaie A (2006) Application of Intelligent Systems for Generating Wireline Logs. Earth Science Journal, School of Geology and Geophysics, University of Oklahoma, 2006 Edition. P.56-66.
9. Kadkhodaie A, Rezaee MR Moallemi SA (2006) A fuzzy logic approach for the estimation of permeability and rock types from conventional well log data: an example from the Kangan reservoir in Iran Offshore Gas Field, Iran. Journal of Geophysics and Engineering, UK, Vol. 3, pp 356-369.
10. Chiu S (1995) Extracting fuzzy rules for pattern classification by cluster estimation. Proc. 6th Int. Fuzzy Systems Association Congress (IFSA '95), Sao Paulo, Brazil, 2, 273-276.
11. Chiu S (1997) Fuzzy Information Engineering: A Guided Tour of Applications (Chapter 9), John Wiley & Sons.
12. Nikravesh M, Aminzadeh, F (2003) Soft computing and intelligent data analysis in oil exploration, Part 1: Introduction: fundamentals of soft computing. 744 pp. Elsevier, Berkeley, USA.
13. Lim JS (2005) Reservoir properties determination using fuzzy logic and neural networks from well data in offshore Korea. Journal of Petroleum Science and Engineering 49 182–92.
14. Labani MM, Kadkhodaie A Salahshoor K (2010) Estimation of NMR log parameters from conventional well log data using a committee machine with intelligent systems: a case study from the Iranian part of the South Pars gas field, Persian Gulf Basin. Journal of Petroleum Science and Engineering, vol. 72, 175-185.
15. POGC report (2003) South Pars gas field geological study. Prepared by Tehran Energy Consultant (TEC), (unpublished report)
16. Kamali MR, Mirshady AA (2004) Total organic carbon content determined from well logs using Δ log R and neuro-fuzzy techniques. J. Pet. Sci. Eng. 45, 141–148.
17. Kadkhodaie A, Rahimpour-Bonab H, Rezaee MR (2009a) A Committee Machine with Intelligent Systems for Estimation of Total Organic Carbon Content from Petrophysical Data: An Example from the Kangan and Dalan Reservoirs in South Pars Gas Field, Iran. Computers & Geosciences, Elsevier Publications, Vol. 35, 459-474.
18. Kadkhodaie A, Rezaee MR, Rahimpour-Bonab H, Chehrazi A (2009b) Petrophysical data prediction from seismic attributes using committee fuzzy inference system. Computers & Geosciences, Vol. 35, 2314-2330.
19. Sugeno, M (1985) Science Pub. Co.Industrial applications of fuzzy control, Elsevier .
20. Mamdani EH (1976) Advances in the linguistic synthesis of fuzzy controllers. International Journal of Man-Machine Studies 8, 66 9–678.
21. Mamdani EH (1977) Applications of fuzzy logic to approximate reasoning using linguistic synthesis. IEEE Transactions on Computers 26, 1182–1191.
22. Larsen PM (1980) Industrial applications of fuzzy logic control. International Journal of Man-Machine Studies 12, 3–10

23. Oppner FH (2002) Speeding up fuzzy c-means: using a hierarchical data organisation to control the precision of membership calculation. Elsevier, Fuzzy Sets and Systems 128, 365-376.

24. Kadkhodaie, A., Takahashi Monteiro S, Ramos F, Hatherly P, et al. (2010) Rock Recognition from MWD Data: A Comparative Study of Boosting, Neural Networks and Fuzzy Logic. IEEE Transactions Letters (GSRL Geosciences and on Remote Sensing), Vol. 7, No. 4, 680-684.

25. Zoveidavianpoor M, Samsuri A, Shadizadeh SR (2012) Adaptive Neuro Fuzzy Inference System for Compressional Wave Velocity Prediction in a Carbonate Reservoir. Journal of Applied Geophysics. 89(2):96-107. doi:10.1016/j.jappgeo.2012. 11.010."

26. Zoveidavianpoor M (2014) A Comparative Study of Artificial Neural Network and Adaptive Neuro Fuzzy Inference System for Prediction of Compressional wave velocity Neural Network and Applications. 25(5):1169-1176. doi:10.1007/s00521-014-1604-2.